การตรวจสอบความบกพร่องเชิงโครงสร้างในชั้นบัฟเฟอร์ InGaAs ที่ปลูกผลึกลงบน GaAs
ด้วยกล้องจุลทรรศน์อิเล็กตรอนชนิดส่องผ่าน

นางสาวพรสิริ คงแจ้ง

INVESTIGATION OF STRUCTURAL DEFECTS IN InGaAs BUFFER LAYERS
GROWN ON GaAs BY TRANSMISSION ELECTRON MICROSCOPY

Miss Pornsiri Kongjaeng

A Thesis Submitted in Partial Fulfillment of the Requirements
for the Degree of Master of Science Program in Physics
Department of Physics
Faculty of Science
Chulalongkorn University
Academic year 2006
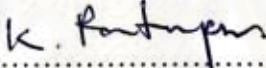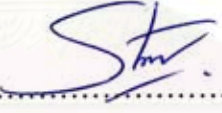
491601

Thesis Title   INVESTIGATION OF STRUCTURAL DEFECTS IN InGaAs
                BUFFER LAYERS GROWN ON GaAs BY TRANSMISSION
                ELECTRON MICROSCOPY
By   Miss Pornsiri Kongjaeng
Field of study Physics
Thesis Advisor Sakuntam Sanorpim, Ph.D.

Accepted by the Faculty of Science, Chulalongkorn University in Partial Fulfillment of the Requirements for the Master's Degree

…………………………………… Dean of the Faculty of Science

(Professor Piamsak Menasveta, Ph.D.)

THESIS COMMITTEE

…………………………………….. Chairman

(Assistant Professor Kiranant Ratanathammapan)

……………………………………… Thesis Advisor

(Sakuntam Sanorpim, Ph.D.)

…………………………………….. Member

(Chanwit Chityuttakan, Ph.D.)

…………………………………….. Member

(Varagorn Hengpunya, Ph.D.)

iv

พรสิริ คงแจ้ง: การตรวจสอบความบกพร่องเชิงโครงสร้างในชั้นบัฟเฟอร์ InGaAs ที่ปลูก
ผลึกลงบน GaAs ด้วยกล้องจุลทรรศน์อิเล็กตรอนชนิดส่องผ่าน (INVESTIGATION OF
STRUCTURAL DEFECTS IN InGaAs BUFFER LAYERS GROWN ON GaAs BY
TRANSMISSION ELECTRON MICROSCOPY)
อ. ที่ปรึกษา: ดร. สกุลธรรม เสนาะพิมพ์, 70 หน้า.

ผู้วิจัยใช้กล้องจุลทรรศน์อิเล็กตรอนชนิดส่องผ่าน (TEM) ตรวจสอบสมบัติทางโครงสร้าง
ในระดับไมโครของชั้นบัฟเฟอร์อินเดียมแกลเลียมอาร์เซไนด์ (InGaAs) ที่เตรียมด้วยกระบวนการที่
แตกต่างกันสี่แบบด้วยวิธีเมธทอลออแกนิกเวเปอร์เฟสอิพิแทกซี (MOVPE) ผลการเปรียบเทียบแสดง
ให้เห็นว่าชั้นบัฟเฟอร์ InGaAs ที่ปลูกผลึกลงบนชั้น InGaAs ที่เตรียมแบบเชิงเส้น (LG-InGaAs) แบบ
ขั้นบันได (SG-InGaAs) และแบบแทรกชั้นซุปเปอร์แลตทิซ (SLS-InGaAs/GaAs) มีคุณภาพสูงกว่า
ชั้นบัฟเฟอร์ InGaAs ที่ปลูกผลึกลงบนแกลเลียมอาร์เซไนด์ (GaAs) โดยตรง จากผลการตรวจสอบ
โดยภาพตัดขวางกล้องจุลทรรศน์อิเล็กตรอนชนิดส่องผ่านแสดงให้เห็นถึงการเกิดดิสโลเคชัน (มิสฟิต
เทรดดิ้งดิสโลเคชันและดิสโลเคชันแบบผสม) ในบริเวณชั้น InGaAs ที่เตรียมแบบเชิงเส้นและแบบ
ขั้นบันได การเกิดดิสโลเคชันในบริเวณชั้น InGaAs ที่เตรียมแบบเชิงเส้นและแบบขั้นบันไดนั้นแสดงให้
เห็นว่าได้เกิดความผ่อนคลายเนื่องจากความแตกต่างของค่าคงที่โครงผลึกระหว่าง InGaAs และ
GaAs แต่จากการตรวจสอบชั้นบัฟเฟอร์ InGaAs ที่ปลูกผลึกลงบนชั้นซุปเปอร์แลตทิซของ
InGaAs/GaAs พบดิสโลเคชันความหนาแน่นสูงในบริเวณชั้นซุปเปอร์แลตทิซและลดลงในชั้นบัฟเฟอร์
InGaAs ตามลำดับ การลดลงของความหนาแน่นของดิสโลเคชันแสดงให้เห็นว่าชั้นซุปเปอร์แลตทิซ
สามารถกรองเทรดดิ้งดิสโลเคชันได้ นอกจากนี้จะอภิปรายเปรียบเทียบความผ่อนคลายความเครียด
ระหว่างชั้นบัฟเฟอร์ InGaAs ที่ปลูกผลึกแบบเชิงเส้น แบบขั้นบันไดและแบบแทรกชั้นซุปเปอร์แลตทิซ
ผู้วิจัยพบว่าเทคนิคการเตรียมชั้นบัฟเฟอร์แบบเชิงเส้นมีจุดเด่น ทำให้เกิดการผ่อนคลาย
โดยการก่อเกิดของมิสฟิตดิสโลเคชัน ในขณะที่การเตรียมโดยการแทรกชั้นซุปเปอร์แลตทิซสามารถ
กรองเทรดดิ้งดิสโลเคชันได้ ดังนั้นผู้วิจัยนำเสนอการเตรียมชั้นบัฟเฟอร์ InGaAs ที่มีการผ่อนคลาย
ความเครียดของโครงผลึกสูง โดยการประยุกต์ใช้กระบวนการเตรียมแบบเชิงเส้นและแบบการแทรก
ชั้นซุปเปอร์แลตทิซร่วมกัน นอกจากนี้ผู้วิจัยได้แสดงผลการใช้บัฟเฟอร์ InGaAs เป็นซับสเตรตสำหรับ
การปลูกผลึกฟิล์มบาง InGaAsN โดยสามารถปรับปรุงคุณสมบัติเชิงแสงและเชิงโครงสร้างให้มี
คุณภาพสูงขึ้นได้และเหมาะสมต่อการนำไปประดิษฐ์เป็นอุปกรณ์อิเล็กทรอนิกส์เชิงแสง เช่น เลเซอร์
ไดโอดและเซลสุริยะแบบมัลติจังชัน

ภาควิชา ....ฟิสิกส์............	ลายมือชื่อนิสิต.........พรสิริ คงแจ้ง..........
สาขาวิชา............ฟิสิกส์............	ลายมือชื่ออาจารย์ที่ปรึกษา..............................
ปีการศึกษา ....2549..............	

4772390323: MAJOR   PHYSICS

KEY WORDS: TRANSMISSION ELECTRON MICROSCOPY/ InGaAs BUFFER LAYERS/ STRUCTURAL DEFECTS / METALORGANIC VAPOR PHASE EPITAXY

PORNSIRI KONGJAENG: INVESTIGATION OF STRUCTURAL DEFECTS IN InGaAs BUFFER LAYERS GROWN ON GaAs BY TRANSMISSION ELECTRON MICROSCOPY. THESIS ADVISOR: SAKUNTAM SANORPIM, Ph.D., 70 pp.

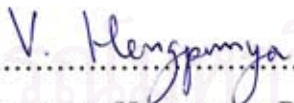Transmission electron microscopy (TEM) investigation have been carried out on the microstructure of InGaAs buffer layers grown on GaAs (001) substrates using four different strategies via metalorganic vapor phase epitaxy (MOVPE). As compared with the quality of InGaAs layer grown on directly GaAs substrate, the growth on linearly-graded InGaAs (LG-InGaAs), step-graded InGaAs (SG-InGaAs) and stain-layer superlattice InGaAs/GaAs (SLS-InGaAs/GaAs) yielded good structural quality buffer layers. The number of dislocations (misfit, threading and mixed dislocations) investigated by cross-sectional TEM was found to be reduced in the InGaAs buffer layers. The generation of dislocations was found to be dominated in the graded regions. This means that the LG-InGaAs and SG-InGaAs layers were relaxed due to the large lattice-mismatch between InGaAs and GaAs, resulting in generation of a large number of dislocations. On the other hand, for the InGaAs buffer layer on SLS-InGaAs/GaAs, a high density of dislocations was observed in the superlattice regions. In fact, density of dislocations was decreased in the InGaAs buffer layer grown on the InGaAs/GaAs superlattice. This demonstrates that the strained-layer superlattice exhibits some filtering of threading dislocations. Also, the strain-relaxation will be discussed in comparison between the InGaAs buffer layers on GaAs, LG-InGaAs, SG-InGaAs and SLS-InGaAs/GaAs.

We found that the grading technique has the advantage of spreading MDs with depth throughout the InGaAs layer and must achieve full relaxation. On the other hand, the SLS technique can be some filtering of TDs. Thus, we suggest that a combination of the LG and SLS techniques is a promising method to achieve high-quality strain-relaxed InGaAs buffer layers for the large lattice-mismatched system. We also show that the use of the InGaAs pseudo lattice-matched substrate is an effective method to fabricate a thick lattice-matched InGaAsN layers with higher optical and structural qualities necessary for the development of the optoelectronic devices such as semiconductor lasers and multijunction (MJ) solar cells.

Department.......Physics........   Student's signature....ทริริ....ณหริง.....
Field of study....Physics........   Advisor's signature.............ว่า.........
  Academic year....2006..........

Acknowledgement

I would like to sincerely express my gratitude to my advisor, Dr. Sakuntam Sanorpim for his valuable suggestions and reassurance in this work. He gave me good experience, such as working with good advice, participating in an international conference (presentation) in Japan, and English writing (journal and thesis).

I would like to thank Assistant Professor Kiranant Ratanathammapan, Dr. Chanwit Chityuttakan, and Dr. Varagorn Hengpunya for serving as chairman and committee, respectively. Their comments on this thesis are also greatly appreciated.

I would like to thank the Advanced Materials Physics Research Group (AMPRG), Semiconductor Physics Research Laboratory (SPRL) and National Metal and Materials Technology Center (MTEC) for facilities in using instrument making this thesis. I wish to thank Assistant Professor Dr. Sukkaneste Tungasmita for useful suggestion my work.

I would like to acknowledge the financial supports from the Thailand-Japan Technology Transfer Project-Overseas Economic Cooperation Fund (TJTTP-OECF) and Graduate Schools of Chulalongkorn University for paying fund for this thesis. I would like to acknowledge Department of Physics, Faculty of Science, Chulalongkorn University for providing teaching. Special thank goes to Professor Dr. Kentaro Onabe, Department of Advanced Materials Science, Graduate Schools of Frontier Science, The University of Tokyo, Japan for providing the great samples and financial supports presentation in Japan.

I would like to thank my friends, Panatda Panperh, Pawinee Klangtakai, Dares Kaewket and my senior for useful discussion and joyful moment. Special thanks go to Siripen Suandon and Pattira Haumhoun for helpful in this work.

Lastly, I would like to sincerely thank my family; my father, my mother and my brother for love, understanding, supports and everything. Important I thanks to Gods for relied on my heart.

Table of Contents

List of Tables

List of Figures

CHAPTER I

INTRODUCTION

1.1 Motivation: Why InGaAs Buffer Layer?

One of the key problems in the fabrication of high-quality semiconductor epitaxy, such as heterostructures and quantum well structures, is the need to achieve abrupt and smooth interfaces. Relaxed buffer layers are required in semiconductor epitaxy to obtain an in-plane lattice-constant, which matches to those of the epitaxial layers (films), different from those available on high-quality large area commercial substrates such as Si, GaAs and InP. This allows the effective misfit between the epitaxial layer and the substrate to be lowered and avoids strain-induced roughening and plastic relaxation of the epitaxial grown layer. As a result, the relaxed buffer layer prevents the growth of defect-free heterostructures. Furthermore, limitation of the band-engineering, which is due to the lattice-constant of the available substrates such as GaAs, Si and InP, can be overcome by growing the relaxed buffer layers, which are designed to accommodate the lattice misfit while confining dislocations far from the buffer layer interface [1].

The state of the art for semiconductor buffer layers is represented by epilayer alloys grown by grading the composition in order to achieve a depth distribution of the lattice parameter. The original idea [2-4] was to keep the surface strain during growth below the critical value which determines the regime of three-dimensional growth [5, 6] and, therefore, which is favorable to the proliferation of threading dislocation (TD) [7]. Several strategies for fabrication of the semiconductor buffer layers have been identified in the literature including simple constant composition layers (CL), linearly-graded layers (LGL), step-graded layer (SGL) [8], and more complicated structures including, for an example, strained-layer superlattice (SLS) [9]. Some explanations of strain relaxation in the buffer layer have been proposed in the literature (Dunstan *et al.* [10] and Tersoff [11]). They focused mainly on the relationship between strain relaxation and composition grading rate in the linear graded InGaAs buffer layer grown on the GaAs substrate. However, no systematic
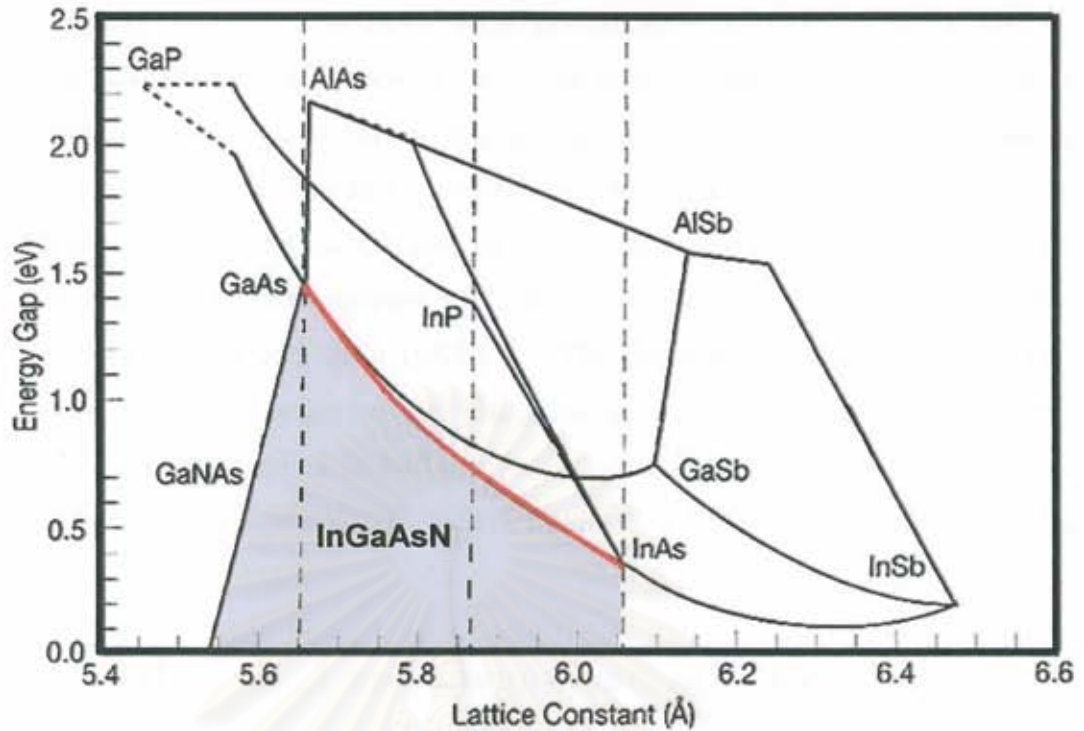
Figure1.1 The relationship between lattice constant and energy gap of binary compound semiconductors (the red line related to $In_xGa_{1-x}As$).

study has been reported in which these different strategies are properly compared. It is still unclear how the different strategies should perform. Linearly-graded (LG) structure, step- graded (SG) structure and strained-layer superlattices (SLS) structure are the simplest ways of controlling the misfit at the growth surface. All structures reduce the TD density compared with single high mismatch constant-composition layers.

$In_xGa_{1-x}As$ pseudo-substrates have a potential impact on the realization of nitride-based optoelectronic devices at room temperature upon optimization of the device structures [12]. Thus, our aim is focused on the $In_xGa_{1-x}As$ buffer layers used as a pseudo-substrate for dilute $In_xGa_{1-x}As_{1-y}N_y$ quaternary alloy, which is of interest for potential use in the 1.3-1.55 μm quantum well (QW) lasers [13] and ultra-high-efficiency tandem solar cells [14] owing to the tunable bandgap while keeping the lattice constant to match with GaAs. However, the large incorporation of N and In required for the bandgap smaller than 1.0 eV leads to the degradation of the structural and optical qualities due to the small solid solubility of N into InGaAs [15, 16] especially when the N concentration exceeds 3%. Therefore, InGaAs pseudo-

substrates with the large lattice constants are attractive for decreasing bandgap of InGaAsN without degradation of the crystal quality. Figure 1.1 shows the relationship between the lattice constant and energy gap for binary compound semiconductors. It is clearly seen that the lattice constant of the dilute InGaAsN quaternary alloy is between those of the GaNAs and InGaAs ternary alloys (shadow area). It is known that InGaAs has face-centered cubic structure (fcc) with lattice constants between GaAs (5.653 Å) and InAs (6.058 Å). This indicates that the lattice constant of $In_xGa_{1-x}As$ is wide range between GaAs and InAs (red line). This dominant feature of $In_xGa_{1-x}As$ was applied to buffer layer as pseudo-substrate for InGaAsN and other large lattice-mismatch systems such as InP/InGaAs on GaAs, as seen in Figure.1.1.

1.2 Objectives and Organization of the Thesis

Although some work on the investigation of semiconductor buffer layers have been carried out as described above, comparison results between the four different growth strategies have not been obtained yet and it is still unclear how the different growth strategies should be carried out. The purpose of this work is to investigate structural properties of the four types of InGaAs buffer layers grown on GaAs (001) substrates with different growth strategies as well as grading profiles using transmission electron microscopy (TEM). The relationships among surface morphology, misfit dislocation (MD) and TD distribution, and strain relaxation are then investigated for different growth strategies. This leads to a simple explanations of strain relaxation specifically related to graded composition profiles. Furthermore, the effectiveness of the lattice-matched InGaAs pseudo-substrate (InGaAs pseudo-substrate) in improving material quality of large lattice-mismatched, high In-content $In_xGa_{1-x}As_{1-y}N_y$ on GaAs (001) by metalorganic vapor phase epitaxy (MOVPE) will also be mentioned.

We focus primary on the following 2 topics: (i) structural investigation and (ii) comparison of the crystalline quality of the four types of InGaAs buffer layers, which are described as follows.

1. $In_xGa_{1-x}As$ constant buffer layer (CL-InGaAs) on GaAs: the CL-InGaAs was grown on GaAs with a constant In composition (x).

2. $In_xGa_{1-x}As$ buffer layer on linearly-graded $In_xGa_{1-x}As$ layers (LG-InGaAs): LG-InGaAs part was obtained by linear grading the In content of the $In_xGa_{1-x}As$ layer from zero up to some final composition x_f [17]. The top of the graded part consists of $In_xGa_{1-x}As$ layer (normally 1 μm thick) with a constant In composition or constant composition buffer equal to the maximum In content in the graded part.

3. $In_xGa_{1-x}As$ buffer layer on step-graded $In_xGa_{1-x}As$ layers (SG-InGaAs): SG-InGaAs were fabricated using the three-step graded type of structure. The top of the system consists of a thick $In_xGa_{1-x}As$ cap layer of final composition x_f.

4. $In_xGa_{1-x}As$ buffer layer on $In_{2x}Ga_{1-2x}As/GaAs$ strained-layer superlattice (SLS): $In_{2x}Ga_{1-2x}As/GaAs$ SLS is grown between the GaAs substrate and a top $In_xGa_{1-x}As$ layer with a constant In composition. The buffer structure consists of a 60-period SLS layer with a fixed nominal value of well thickness (L_Z) 10 nm for the $In_{2x}Ga_{1-2x}As$ wells and barrier thickness (L_B) 10 nm for the GaAs barriers.

Note that all of the InGaAs buffer layers are grown on GaAs (001) substrates by MOVPE under the same growth conditions, such as growth temperature and growth pressure.

This thesis is organized as follows.

Chapter 2: Epitaxy growth and the structural defects such as point, line, planar and bulk defects which are generated in epitaxial layers especially generation of line defects or dislocations are described. In addition, the growth of dislocation-free epitaxial layer is described. Investigation methods, including high resolution X-ray diffraction (HRXRD) and transmission electron microscopy (TEM), are described. Further, the analytical theory of the image mode TEM and the preparation of specimens for the cross-sectional TEM are described in details.

Chapter 3: Metalorganic vapor phase epitaxial (MOVPE) growth information and the structures of the four types of InGaAs buffer layer used in this study are explained. Initial investigated results, such as composition, surface morphology and strain relaxation in all the InGaAs buffer layers, are presented in details.

Chapter 4: Microstructural investigation of CL-InGaAs, LG-InGaAs, SG-InGaAs and SLS-InGaAs/GaAs buffer layers are carried out by TEM, focusing

particularly on the generation of line defects, namely dislocations. In addition, a comparison result of micro-structural properties between the four types of InGaAs buffer layers is discussed.

Chapter 5: To test the quality of the InGaAs pseudo-substrates, the InGaAsN layers grown on the lattice-matched InGaAs pseudo-substrates are investigated using various investigation methods. Strain and microstructural properties of the InGaAsN layer on the lattice-matched InGaAs pseudo-substrate are discussed in comparison to the InGaAsN layer grown directly on the GaAs substrate.

Finally, the conclusion of this thesis is given in Chapter 6.
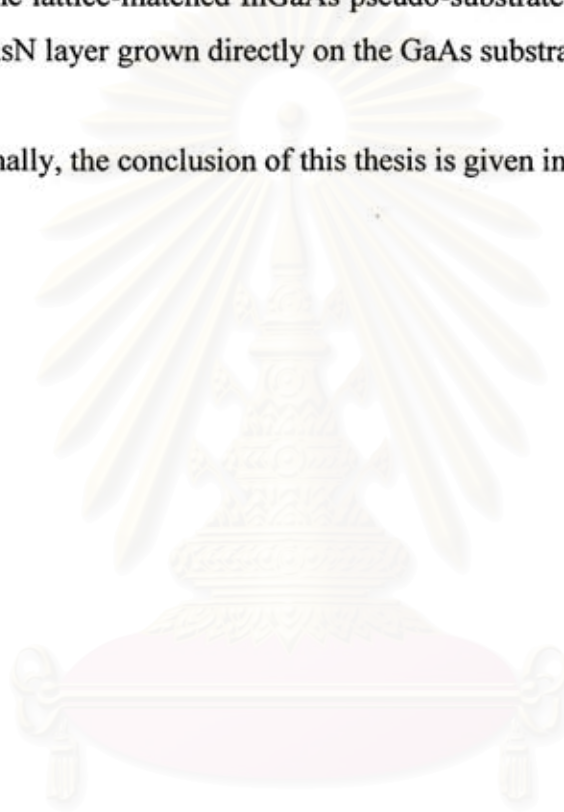
CHAPTER II
HETEROEPITAXY: DISLOCATIONS
AND CHARACTERIZATION

This chapter will briefly present strain in the context of semiconductor heterostructures in order to understand the strained heteroepitaxy. Especially, the strained behavior related to the dislocation mechanism which is important parameters of this work will be discussed. Also, the experimental details are explained in this chapter. It consists of two main characterization methods: high resolution X-ray diffraction and transmission electron microscopy, which are used to analyze the alloy composition and the feature of dislocations, respectively.

2.1 Heteroepitaxy

Epitaxy is a kind of interface between a thin film and a substrate. The term epitaxy (greek; "epi" means "placed or resting upon" and "taxis" means "arrangement") describes an ordered single-crystalline film growth on the top of a single-crystalline substrate. The word epitaxy was apparently introduced into the literature by the French mineralogist L. Royer in 1928 [18]. The epitaxial growth can be divided two types which are homoepitaxy and heteroepitaxy. Homoepitaxy refers to growth of a single-crystalline film on a substrate of the same semiconductor material, such as Si film on Si substrate. In this case, the epilayer generally exhibits free of defects and high structural quality. Another type of epitaxy is heteroepitaxy and refers to the growth of semiconductor crystals of a certain material on the crystal of another material, such as InGaAs film grown on GaAs substrate. Figure 2.1 shows schematically the illustration of the differences of three types of heteroepitaxy. Homoepitaxy is structurally very similar to the lattice-matched heteroepitaxy that the epitaxial layer and the substrate have very small different lattice parameter, as shown in Figure 2.1 (a). In this case, the epitaxial layer with arbitrary thickness can be grown without any structural defects, especially misfit dislocation. For small misfit,
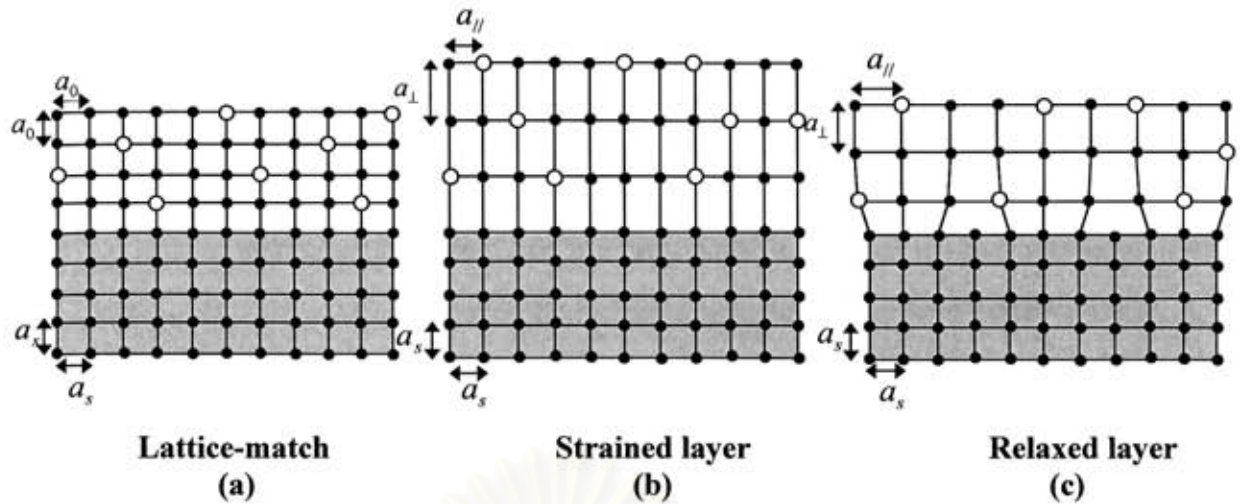
Figure 2.1: Schematic illustration of (a) lattice-matched heteroepitaxy, (b) strained lattice-matched heteroepitaxy, and (c) relaxed lattice-mismatched heteroepitaxy.

as shown in Figure 2.1 (b), an overlayer will deform elastically to match the in-plane lattice constant ($a_{//}$) of the substrate. Under the compressive strain, $a_{//}$ is forced to shrink and the perpendicular lattice constant ($a_{\perp}$) is expanded. Likewise, the overlayer with lattice constant smaller than that of the substrate will be in tension within the plane and compression normal to the planes. Such layers are called strained lattice-matched heteroepitaxy. On the other hand, at certain layer thickness, namely "critical thickness", the overlayer becomes energetically favorable to reduce strain by introduction of misfit dislocations [12], which allows the epilayer to relax toward its free lattice constant, as shown in Figure 2.1 (c). In fact, an effect of strain relaxation is a generation of several kinds of crystal defects, such as dislocations, stacking faults and twins, which affects the lattice constant of the overlayer ($a_{\perp} = a_{//} \neq a_s$).

2.2 Dislocations

2.2.1 Defect types

Normally, types of crystal defects are usually classified according to their dimensions. Zero-dimensional defects are point defects which are vacancies and interstitials. Vacancy is produced to remove one atom from the lattice and place it on the surface of the crystal and/or the interstitial site. Interstitial is created by removing one atom from the surface and inserting it into an interstitial site. All the point defects mentioned produce local distortion in the otherwise perfect lattice. For one-

dimensional defects or line defects, it is called dislocations which some of atoms of the crystal lattice are misaligned. The presence of dislocations is resulting from the lattice-strain (distortion). The phenomena of generation dislocation will be described in detail in the Sections 2.2.2 and 2.2.3. The third type is two dimensional or planar defects which consist of stacking faults, grain boundaries and twin boundaries etc. A stacking fault concerns with a disturbance in the regularity of the stacking of planes of atoms in a crystal lattice. This usually occurs when a plane is inserted into or removed from the lattice. The insertion of an extra plane in the stacking is known as an extrinsic stacking fault, while the removal of plane is referred to an intrinsic stacking fault. For example, the stacking sequences of body-centered or face-centered cubic lattice along the <111> orientations is *ABCABCABC*.... but the change in sequence resulting from intrinsic stacking fault with new sequence *ABCBCABC*.... A grain boundary refers to the transition region or interface between crystals whose atomic arrangements are different in orientation with respect to each other. Finally, twin is planar defect where a mirror image of the regular lattice is formed during the growth. The twin boundary is the mirror plane of the twin formation. The last type of crystal defect is three-dimensional or bulk defects which include voids and precipitates. Voids are small areas where there are no atoms and can be thought of as clusters of vacancies. Impurities can cluster together to form small regions of a different phase. These are often called precipitates. The crystal defects have important effects on the properties of the crystalline materials.

2.2.2 Generation of dislocations

Dislocations are line defects and in the locality of the dislocation the atoms are displaced from their position in the ideally perfect lattice. When the single crystals are plastically deformed, dislocations move under the applied shear stress so that the dislocation line represents a boundary between the unslipped and slipped areas on the slip planes. The shear stress required for this process was first calculated by Frenkel in 1962. Figure 2.2 is an illustration of atom positions used to estimate critical shear stress for slip. It is assumed that there is a periodic shearing force required to move the top row of atoms across the bottom row which is given by
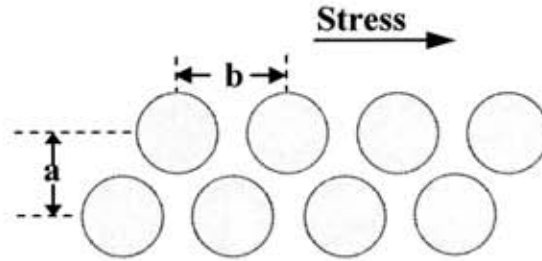
Figure 2.2: Atom positions used to estimate critical shear stress for slip.

$$\tau = \frac{Gb}{2\pi a} \sin \frac{2\pi x}{b} \tag{2.1}$$

where τ is the applied shear stress, G is the shear modulus, b the spacing between atoms in the direction of the shear stress, a the spacing between the rows of atoms and x the shear translation of the two rows away from the low-energy equilibrium position [19]. In the experiment, there are evidences for generation of dislocations in the films. It was found that, two mechanisms of dislocation generation are (i) active during growth when the highly lattice-mismatch occurred strain relaxation by introduction of misfit dislocations (MDs) at film-substrate interfaces (Figure 2.1 (c)) and (ii) post-growth dislocations which are generated behind the growth, such as during growth-temperature quenching to room temperature [20], or other thermal treatments. Then, the crystals have dislocations which are usually inclined to the growth surface and which will be propagated in the strained lattice-matched layer in the same direction as in the substrate. Such dislocations are known as threading dislocation.

Generally, there are two basic types of dislocation, namely the edge and the screw dislocations. Besides, mixed dislocation combining aspects of both types are also common. An edge dislocation may be described as an extra half-plane of atoms inserted in the perfect crystal, as illustrated in Figure 2.3 (a), resulting in that part of the lattice containing extra atoms and the rest of the lattice containing the correct number of atoms. The dislocation line of an edge dislocation is the line connecting all the atoms at the end of the extra half-plane. If we describe a clockwise loop around the edge dislocation, starting at point x and going an equal number of atoms spacing in each direction, we finish one atom spacing from starting at point y. The vector required to complete the loop is the Burgers vector (b). In this case, the burgers vector
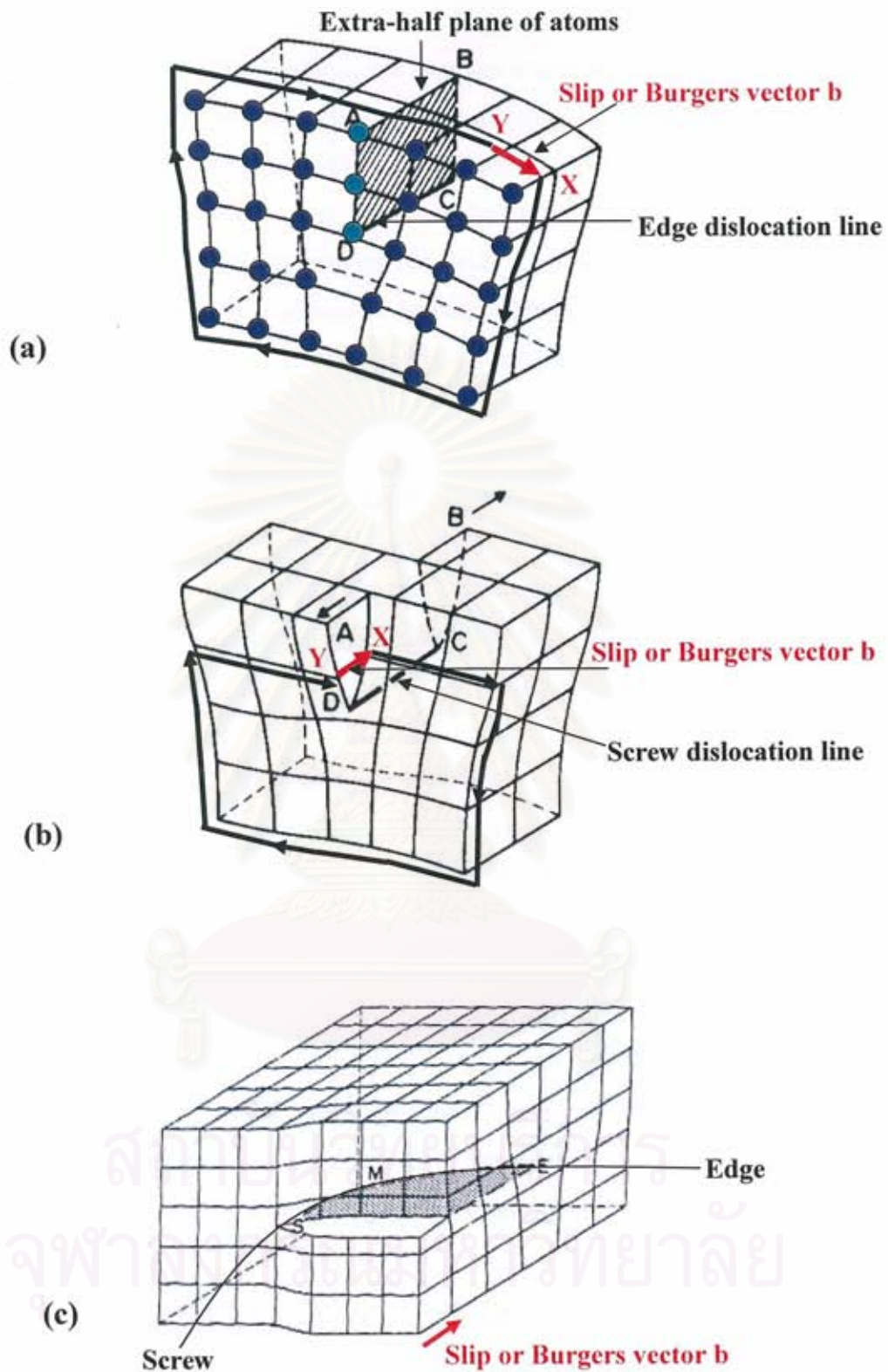
Figure 2.3: Schematic illustration of (a) edge dislocation, (b) screw dislocation and (c) mixed dislocation where *b* represents the Burgers vector [19].

is perpendicular to the dislocation line. If the dislocation is such that a step or spiral ramp is formed by the displacement of atoms in a plane in the crystal lattice, then it is referred to as a screw dislocation. Screw dislocation exhibits a helical path is traced around the dislocation line, as shown in Figure 2.3 (b). In this case, Burgers vector is parallel to the dislocation line. As shown in Figure 2.3 (c), mixed dislocation consists of both edge and screw components, with a transition region between them. The boundary separating the slipped and unslipped regions of the crystal are curved which is mixed dislocation. The burgers vector remains the same for all portions of the mixed dislocation.

2.2.3 MDs and TDs in heteroepitaxial layers

For the heteroepitaxy, there are many models for the generation of MDs and TDs. MDs are associated with TDs and extended into a film growing epitaxially on the substrate. Pure edge MDs are the most efficient at misfit strain. They have been obtained on many heteroepitaxial systems such as SiGe/Si, Ge/GaAs and InGaAs/GaAs with (001)-oriented substrates (Vdovin et al., 1997 [21]). The number of MDs depends on the lattice mismatch, growth thickness, layer composition and the temperature or annealing (Hull and Bean 1989 [22]). MD propagation is accompanied by a shift of dislocations from the interface upwards into the layer or downwards into the substrate. Hongland et al. (2004) [23] reported influence of surface steps on glide of TDs during layer growth. They demonstrated the surface step via the glide of TDs, which is energetically favorable when the thickness of the layer exceeds the critical thickness. The surface steps are seen as 2D arrays so-called crosshatch when we look at from the top as can be observed by atomic force microscopy (AFM) and TEM image as shown in Fig.2.4 (Yastrubchak et al., 2003 [24]).

2.3 Growth of Dislocation-free Layers

The production of dislocation-free single crystal epitaxial layers is currently of considerable interest owing to their applications in the semiconductor and optoelectronic devices industry. Dislocations have been shown to be associated with non-radiative recombination processes [25]. Further, the surface too of epitaxial layer is affected by the presence of dislocations. In the phenomenon of "crosshatching",

(a)

(b)
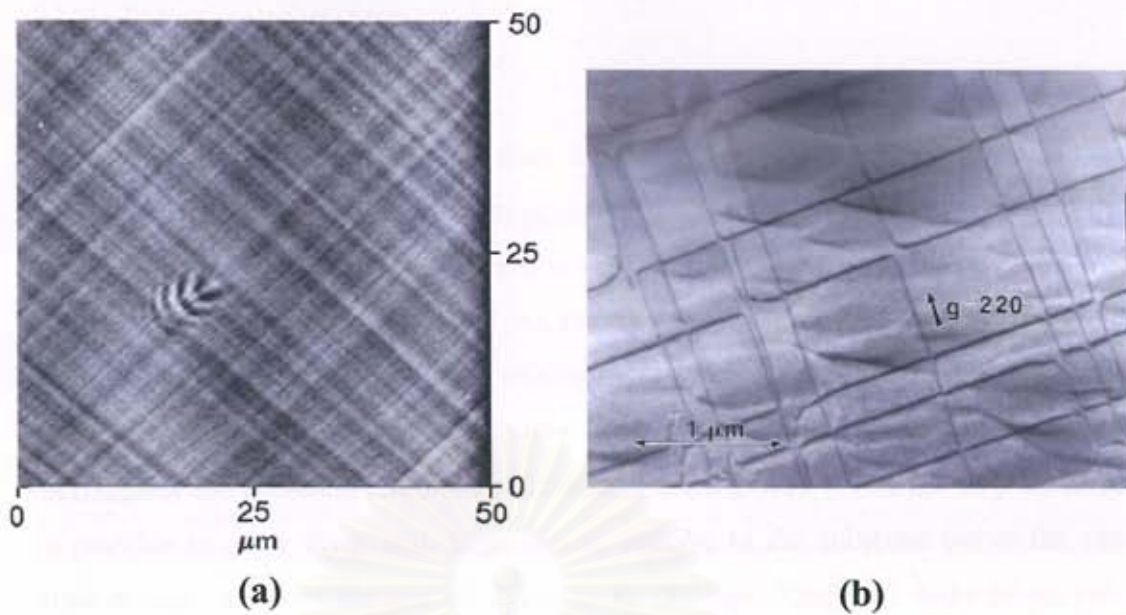
Figure 2.4: (a) AFM micrograph shows a well-defined cross-hatch pattern reproducing the network of misfit dislocations and (b) TEM image of misfit dislocations at the interface of InGaAs/GaAs heterostructure [26].

the surface of the layer shows a crossed pattern of ridges and valleys corresponding to crossed grids of MDs many microns below the surface (Figure 2.4 (a)) [26]. Therefore, it is of some importance for the designer of such epitaxial devices to have an understanding of the factors which governs the generation and subsequent behavior of dislocations in epitaxial single crystal films in order to produce layers with are free of all dislocations, or at least of those which have undesirable properties in certain regions.
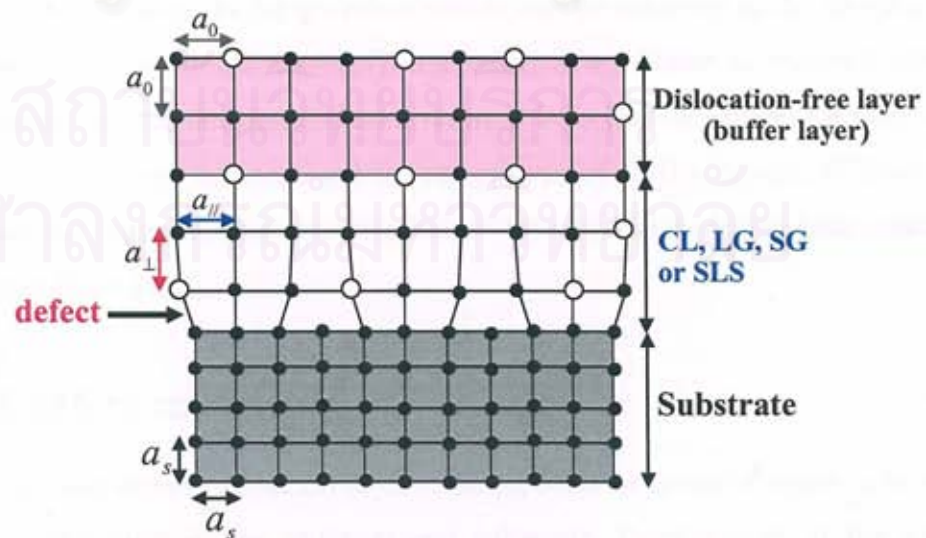
Figure 2.5: Schematic illustration of dislocation-free layers (buffer layer).

2.3.1 Graded layers

The interfaces considered thus far have been abrupt transitions from one crystal to another. However, in many applications, the two crystals are separated by a transition layer in which the composition varies continuously (linearly-grading), or in discrete steps (step-grading), from one crystal type to the other. This configuration may be used to accommodate layer misfits without cracks or other deleterious effects. Theoretical and experimental studies have shown that dislocations generally accompany the accommodation of mismatch in these graded layers [27-29]. However, it possible to grow layer with large misfits relative to the substrate but at the same time obtain very low dislocation densities in the layer itself, all dislocations being confined to the graded regions. Thus, the dislocations are normally required in the graded layers for strain release. As shown in Figure 2.5, it is found that the lattice constant varies with composition until lattice constant of relax layer itself ($a_0 \neq a_{//}, a_\perp$). Then, the growth of the top layer (buffer layers) on the transition layer (graded layer) can be dislocation-free layer. In the production of dislocation-free layers two different types of dislocations must be considered. In the first place substrate-inherited TDs must be eliminated. This may be done by using dislocation-free substrates, or if this is not possible, by wipe out the TDs into a misfit interface. Elimination of TDs which are inclined along the growth direction become bent into the interfacial plane at the next composition step in the graded layers and are thus prevented from propagation into subsequent growth. A high density of misfit dislocations bent normal to the growth direction can be observed at the interface due to the abrupt compositional step [27]. Secondly, if a junction is required with no misfit dislocations, the thickness of the layer must be below the critical thickness. The critical thickness may be increased by the growth of further layers. If large film thicknesses are required, very low misfits are indicated and ideally lattice-matched systems should be used.

2.3.2 Lattice matching

The most effective method of eliminating MDs in epitaxial layers is to match the lattice constants of the epilayer and substrate. Furthermore, if the growth temperature is high, residual strains will present unless the coefficients of thermal

expansion are also matched. This matching is possible by using ternary and quaternary layer of III-V compounds and similar materials [29, 30]. A ternary layer would have the composition $A_xB_{1-x}C$ or AC_yD_{1-y} where A and B are group III elements (Ga, In or Al) while C and D are group V elements (As, P or N). The composition parameters x and y may be varied from zero to unity using suitable growth techniques. The lattice parameter a (x) of ternary compound $A_xB_{1-x}C$ is given by

$$a(x) = xa_{AC} + (1-x)a_{BC} \tag{2.2}$$

where a_{AC} and a_{BC} are the lattice constants of AC and BC respectively. This linear relationship is known as Vegrad's law and is known to hold for ternary compounds. On the other hand, the coefficient of linear thermal expansion α (x) of the ternary compound may also be calculated using Vegrad's law:

$$\alpha(x) = \frac{xa_{AC}\alpha_{AC} + (1-x)a_{BC}\alpha_{BC}}{a(x)} \tag{2.3}$$

where α_{AC} and α_{BC} are the coefficients of linear thermal expansion of AC and BC respectively.

In the case of a quaternary compound of composition $A_xB_{1-x}C_{1-y}D_y$ with A, B, C and D as above, the lattice constant and coefficient of thermal expansion are given by [31]

$$a_{ABCD}(x,y) = (1-x)(1-y)a_{AC} + x(1-y)a_{BC} + (1-x)ya_{AD} + xya_{BD} \tag{2.4}$$

and

$$\alpha_{ABCD}(x,y) = \frac{(1-x)(1-y)a_{AC}\alpha_{AC} + x(1-y)a_{BC}\alpha_{BC} + (1-x)ya_{AD}\alpha_{AD} + xya_{BD}\alpha_{BD}}{a_{ABCD}(x,y)}$$

$$\tag{2.5}$$

where a_{AC}, a_{BC}, a_{AD} and a_{BD} are the lattice constants and α_{AC}, α_{BC}, α_{AD} and α_{BD} are the coefficients of linear thermal expansion of AC, BC, AD and BD, respectively. Not that requirement such as a suitable value of the bandgap must be satisfied as well as lattice constant, and a compromise solution must be found of materials. If, for example, the bandgap differences in coefficients of thermal expansion, the device will be strained at room temperature [30]. The principles given here will be helpful in selecting the best compromise.

2.4 Characterization Methods

2.4.1 High Resolution X-ray Diffraction

High resolution X-ray diffraction is very important experiment technique that has been used to analyze crystal structure of the epitaxial films, including lattice constants and crystal structure, and orientation of single crystal, etc. The monochromator X-ray beam with a specific wavelength (1.5406 Å), a sample state which is capable of movement in different directions, tilt and rotation for precise placement of sample and motorized slit at detector are referred high resolution X-ray diffraction. The diffraction condition can be occurred by according to Bragg's law. Above-mentioned was demonstrated that, the lattice parameters are important for characterization of structural properties such as lattice mismatch, residual strain and strain relaxation etc. In this work the HRXRD technique is used to determine $a_{//}$, $a_{\perp}$ and lattice constant of relax layer (a_0) via the (004) $2\theta/\omega$ scan and the asymmetric reflect (115) ω-scan and $\omega/2\theta$-scan mapping modes. We can derivative composition of the epitaxial layers from lattice constant. Firstly, X-ray rocking curve for (004) symmetrical reflection was measured to determine the value of interplanar spacing, d_{hkl} . It is known that the interplanar spacing d_{hkl} is a function both of the plane indices (*hkl*) and the lattice constants. The exact relation depends on the crystal system involved and for the tetragonal system takes on the relatively simple from

$$d_{hkl} = \frac{a_{//}}{\sqrt{h^2+k^2}} + \frac{a_{\perp}}{\sqrt{l^2}} \qquad (2.6)$$

In this case, the interplanar spacing, $d_{004} = a_{\perp}/4$ results from the (004) plane measurement. Figure 2.6 shows a typical HRXRD (004) $2\theta/\omega$-profile of InGaAs layer on GaAs (001) substrate. The diffraction peaks of InGaAs layer and GaAs were clearly observed at 64.835° and 66.053°, respectively. Then, the interplanar spacing can be calculated by Bragg's law. From the separation between the InGaAs and GaAs reflection peaks, $a_{\perp}$ was estimated to be 5.748 Å. Secondly, we used HRXRD mapping of the (115) reflection to measure the $a_{//}$ of the epilayers. The inclination between the asymmetric plane of the substrate and of the epilayer is observed owing

to a tetragonal distortion. The angle (ψ) between the (001) plane and the (115) plane of the strained layer is given by [32]

$$\psi = \tan^{-1}(\sqrt{2} \cdot a_{\perp} / 5 \cdot a_{//}) \tag{2.7}$$

For the cubic symmetry, such as lattice-matched layers or fully relaxed layers ($a_{//} = a_{\perp}$), thus, ψ becomes a constant value of $\tan^{-1}(\sqrt{2}/5)$. Due to the tetragonal lattice distortion of the strained epilayer ($a_{//} \neq a_{\perp}$), the tilted angle $\Delta\psi$ between the (115) planes of the GaAs substrate and the InGaAs layer is represented by [32]

$$\Delta\psi \equiv \psi_{GaAs} - \psi_{InGaAs} \equiv \psi_0 - \psi_1 = \tan^{-1}(\sqrt{2}/5) - \tan^{-1}(\sqrt{2} \cdot a_{\perp} / 5 \cdot a_{//}) \tag{2.8}$$

Figure 2.7 shows a typical ω-scan and $\omega/2\theta$-scan mapping measured around the asymmetrical (115) reflections. It is found that diffraction peaks from both GaAs (115) and InGaAs (115) planes are directly seen. Separation between the GaAs and InGaAs peaks in ω-axis "$\Delta\omega$" was estimated to be -0.08, which corresponds to the tilted angle $\Delta\psi$ between GaAs (115) and InGaAs (115) planes. From the value of $a_{\perp}$, which was estimated to be 5.748 Å, and using Eq. (2.8), $a_{//}$ was estimated to be 5.719 Å. The next step is to calculate a lattice constant of the relaxed layer (a_{relax}). This is a lattice constant of the free-standing crystal. The lattice constant of the relaxed layer (or free lattice constant) is expressed in terms of elastic stiffness constant (C_{11}, C_{12}):

$$a_{relax} = a_{InGaAs} = \frac{2 \cdot C_{12} \cdot a_{//} + C_{11} \cdot a_{\perp}}{2 \cdot C_{12} + C_{11}} \tag{2.9}$$

To examine the alloy composition (In concentration or x) from the lattice constant of the relaxed layer, here we calculated from Vegrad's law (as described in Section 2.3.2):
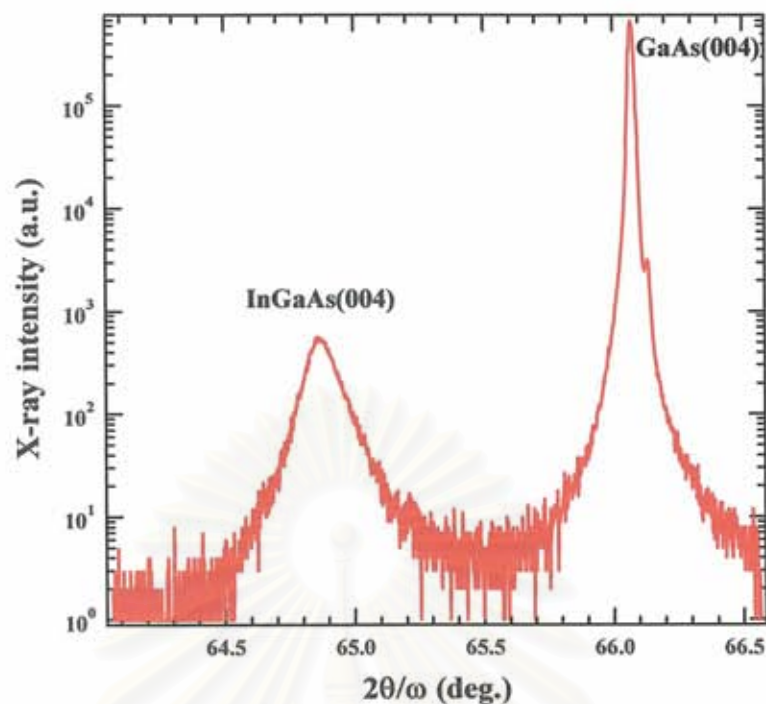
Figure 2.6: A typical High resolution X-ray diffraction (004) $2\theta/\omega$-profile of the InGaAs layer grown on the GaAs (001) substrate.
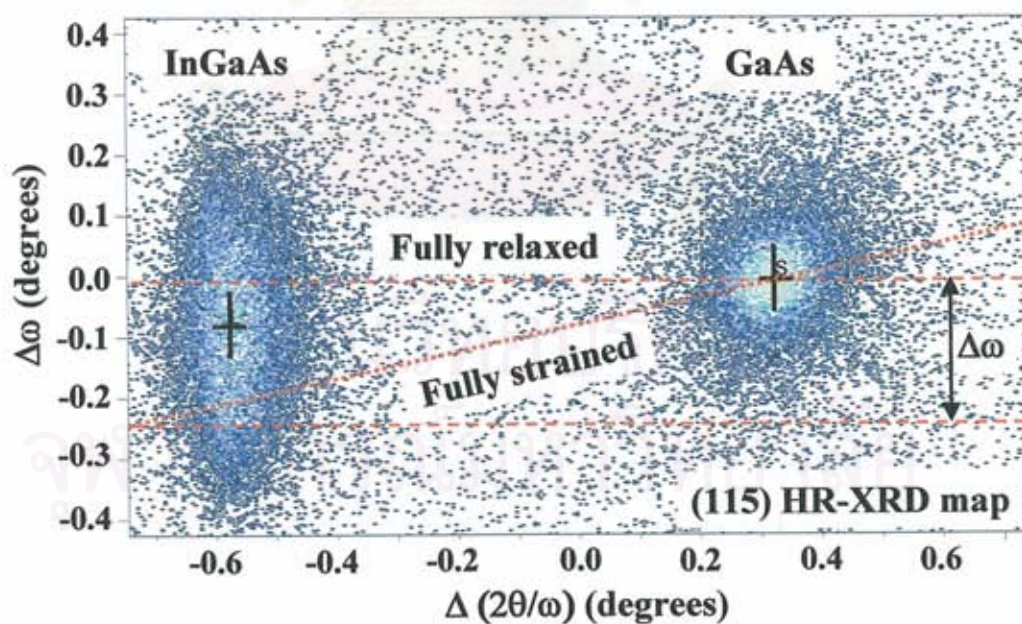
Figure 2.7: Typical (115) High resolution X-ray diffraction map of InGaAs layer grown on GaAs (001) substrate.

$$a_{relax} = a_0 = xa_{InAs} + (1-x)a_{GaAs} \qquad (2.10)$$

Since C_{ij} in Eq. (2.9) are the elastic stiffness constant of the alloy, they have to be averaged depending on the alloy composition. Thus,

$$C_{11} = \frac{xa_{InAs} \cdot C_{11}^{InAs} + (1-x)a_{GaAs} \cdot C_{11}^{GaAs}}{a_0} \qquad (2.11)$$

$$C_{12} = \frac{xa_{InAs} \cdot C_{12}^{InAs} + (1-x)a_{GaAs} \cdot C_{12}^{GaAs}}{a_0} \qquad (2.12)$$

where C_{11} and C_{12} are the elastic stiffness constants of $In_xGa_{1-x}As$. Elastic stiffness constants for the component binary semiconductors are listed in the Table 2.1. In the following, these four equations were used to determine In composition (x) of the $In_xGa_{1-x}As$ epitaxial layer. Firstly, we assume for the elastic stiffness constants of InGaAs as the values of GaAs and $a_\perp$ and $a_{//}$ are calculated from symmetric (004) $2\theta/\omega$ X-ray diffraction scan and asymmetric (115) $\omega/2\theta$ reciprocal space maps, respectively by using Eq. (2.9) to find lattice constant of relax layers. Then, the value of a_{relax} were used to calculate the In content (x) in $In_xGa_{1-x}As$ by using Eq. (2.10). Finally, the calculated x value is used to obtain better approximation for elastic stiffness constants of InGaAs using Eqs.(2.11) and (2.12). In this case, the lattice constant of the relaxed layer (a_{relax}) was estimated to be 5.734 Å. The In concentration in InGaAs layer was $x \cong 20\%$. The elastic stiffness constants of InGaAs were also calculated to be $C_{11} = 11.13$ and $C_{12} = 5.199\ 10^{11}$ dyn/cm^2.

Parameters	GaAs	InAs
a (Å)	5.653	6.058
C_{11} $(10^{11}\,dyn/cm^2)$	11.88	8.329
C_{12} $(10^{11}\,dyn/cm^2)$	5.38	4.526

Table 2.1: Lattice constants and elastic stiffness constants of GaAs and InAs [33].

On the other hand, the lattice mismatch is investigated when we known the lattice constant of the epilayer. In general, the difference in the lattice constant between a film and substrate can be characterized by the lattice mismatch or lattice misfit, f, defined as

$$f = \frac{\Delta a_{//,0}}{a_s} = \frac{(a_{//,0} - a_s)}{a_s} \qquad (2.13)$$

where $a_{//,0}$ are the in-plane and free lattice constant of the epitaxial layer.

a_s is the lattice constant of the substrate.

For the $In_{0.2}Ga_{0.8}As$ epilayer, the values of lattice mismatch of the in-plane and relaxed lattice constant between the layer and substrate were estimated to be 1.168% and 1.433%, respectively. Moreover, we can judge the strain relaxation and the residual strain in the layer. The residual strain in directions of parallel ($\varepsilon_{//}$) and perpendicular ($\varepsilon_{\perp}$) to the substrate surface can be described by following:

$$\varepsilon_{//,\perp} = \frac{a_0 - a_{//,\perp}}{a_{//,\perp}} \qquad (2.14)$$

Higher values of lattice-mismatch effect strain relaxation of the epilayers corresponding to less value of residual strain. The strain relaxation can be interpreted from strain factor, which expressed as,

$$strain\ factor(\%) = \frac{a_0 - a_{//}}{a_0 - a_s} \times 100\% \qquad (2.15)$$

From Eq. (2.15), the strain factor amounts to zero demonstrative fully relaxation. On the contrary, 100% strain factor refers to the fully strained layer. $\varepsilon_{//}$, $\varepsilon_{\perp}$ and strain factor for the $In_{0.2}Ga_{0.8}As$ epilayer were determined to be 0.262%, 0.244% and 18.49%, respectively. To describe the strain relaxation, in Figure 2.7, it is found that the red-dashed and red-dotted lines are calculated by using Eq. (2.8) for fully relaxed and fully strained $In_{0.2}Ga_{0.8}As$ epilayer, respectively. For fully relaxation, the value of $a_{//}$ is equal to that of $a_{\perp}$, showing $\Delta\omega = 0$. For fully strain, the value of $a_{//}$ is equal to that of a_s. In this case, the $In_{0.2}Ga_{0.8}As$ epilayer is completely strained. In addition the broadening of $\Delta\omega$, which indicates the distribution of crystal orientation due to the generation of dislocations, is referred to the relaxation of $In_{0.2}Ga_{0.8}As$ epilayer.
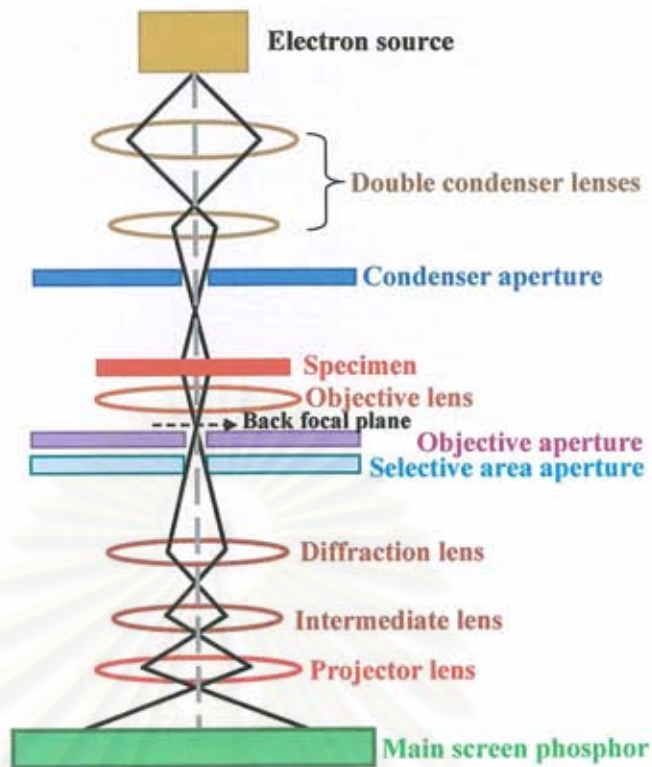
Figure 2.8: Schematic ray diagram of transmission electron microscope [34].

2.4.2 Transmission Electron Microscopy

I. Principle of TEM

Transmission electron microscopy is the technique most widely used for the observation of microstructures of semiconductor thin films, such as crystal structures as well as crystal defects. In our work, TEM is mainly used as a tool for investigation of dislocation mechanisms in the epitaxial layers. The transmission electron microscope can be compared with the optical microscope. In TEM, the light source is replaced by an electron source which produces an electron beam with energy of typically 100-400 kV. Schematic ray diagram for a TEM is shown in Figure 2.8. Electrons emerge from the condenser lenses onto the specimen. Double condenser lenses produced a nearly parallel incident electron beam at the specimen. The scattered electrons are concentrated into discrete directions for a crystalline specimen. These diffracted beams satisfy the requirements of Bragg's condition. Thus, each set of parallel crystal planes diffract electrons in a specific direction. The diffracted electron beams are brought to focus in the back focal plane of the objective lens which is the plane of diffraction pattern. The diffraction lens is focused on the back
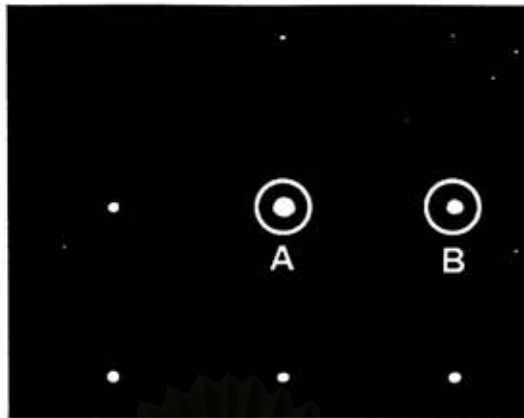
Figure 2.9: Diffraction pattern of diamond silicon showing the relationship between objective aperture and TEM images. The BF and DF image is formed by selecting the direct beam (A) or the diffracted beam (B), respectively.[35]

focal plane and project a magnified diffraction pattern on the main screen phosphor, namely the *diffraction mode*. On the other hand, the objective lens produces an inverted image of the specimen in the first image plane. If the diffraction lens is focused on this plane, the TEM is operated in the *imaging mode,* which is a useful observation for crystal defects. The intermediate lenses are used to magnify this image further and a highly magnified image can be produced on the main screen phosphor. Moreover, a selected area of the specimen, which is interested, produces a selected area diffraction (SAD) pattern by the selective aperture. Due to the use of electron source, TEM system is under vacuum and the specimen must be very thin to allow the electrons to penetrate it which is described later in section of sample preparation. To distinguish the crystal defect types, TEM image mode were performed and analyzed.

In the TEM imaging mode, a diffraction pattern has been obtained first, since the pattern indicates how the electron beam scat in the specimen. Figure 2.9 shows a diffraction pattern from a crystalline material with schematic indication of the location of objective aperture. When the directly transmitted electron beam through the specimen is selected, the display image is called "bright field (BF) image" (spot A). Whereas, when one of the diffracted beams is chosen, the observed image is called "dark field (DF) image" (spot B). The BF and DF images are two basic types to form an amplitude contrast in the TEM micrograph. An amplitude contrast of such images in the TEM will be compounded of mass-thickness contrast and diffraction

Incident
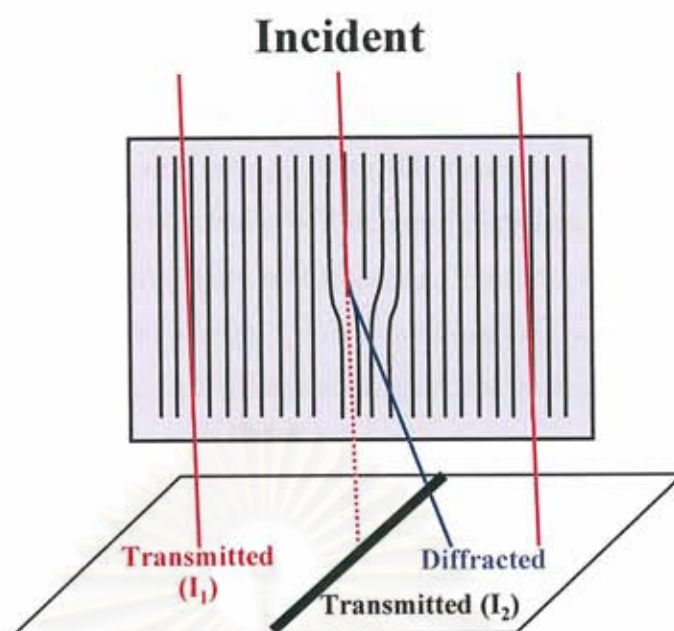
Figure 2.10: Diffraction contrast at plane near an edge dislocation bent into the orientation.

contrast. Mass-thickness contrast is important if we are looking at non-crystalline and/or less uniformity specimens. On the other hand, we are interested the diffraction contrast owing to single-crystalline specimen. "Contrast" is the appearance of a feature in an image. Contrast in BF and DF images is usually "diffraction contrast" or the variations in intensity of diffraction across the specimen. The diffraction contrast is usually clarified as a result of an elastic scattering of electrons from planes of atoms in crystalline material. When electron beams encounters crystalline materials, there is a strong preferential scattering in a certain well-defined direction according to Bragg's condition. The contrast (C) is defined quantitatively in terms of the different in intensity (ΔI) between two adjacent areas. I_1 and I_2 are intensities of the areas 1 and 2, respectively.

$$C = \frac{I_1 - I_2}{I_2} = \frac{\Delta I}{I_2} \qquad (2.16)$$

Diffraction contrast is especially useful to image such crystal defects as dislocations, stacking faults and grain boundaries. For an example of diffraction contrast, a schematic diagram of the dislocation contrast is shown in Figure 2.10. To make dislocations visible in TEM micrograph, the optimum condition is when the orientation of the entire specimen is close to, but not exactly in the Bragg's condition.

In this case, the plane near a dislocation core will be bent locally to satisfy the Bragg's condition. Therefore, this local region of the specimen will diffract the electron beam much more strongly than the adjacent region. The intensity of the directly transmitted electron beam will be reduced and that of the diffracted electron beam increased in column near the dislocation. Then, the dislocation will appear as a dark line in a BF TEM image. On the contrary, the specimen is perfectly flat, uniformly thick and free of structural defects; the image is homogeneous without variations in intensity.

II. Specimen preparation

The cross-sectional specimen for TEM is generally applied to investigate the epitaxial films. For TEM investigation, the specimen is required to be thin enough for electron transmission (<200 nm). Therefore, the preparation method must be carefully taken to obtain the nanometer thickness. The specimen preparation for the cross-sectional TEM is consisted of four steps which are cutting, clamping, polishing and ion milling processes.

Cutting process

In order to remove oil on the specimen surface, before cutting the specimen, the specimen is cleaned with acetone and followed by methyl alcohol. After that the specimen surface is stick on the microscope slide with masking tape and cut the specimen in size of 1×2 mm^2 by a 0.16 mm diamond-wheel saw, as shown in Figure 2.11. This specimen size is selected to match the specimen grid with diameter of 3-mm, which can be contained in the specimen holder for TEM system.

Clamping process

After the cutting process, the specimen surfaces are cleaned again using acetone and followed by methyl alcohol. As shown in Figure 2.12 (a), the clamping process is to stick surfaces of the 2 specimens together with M-BOND 610 glue. Then, clamp the stuck specimens with the clamping holder and then screw the hold up until the 2 specimen surface was tight, as shown in Figure 2.12 (b). After that, the clamping holder was heated using the hot plate at temperature of 80 °C for 24 hours, as shown in Figure 2.12 (c).
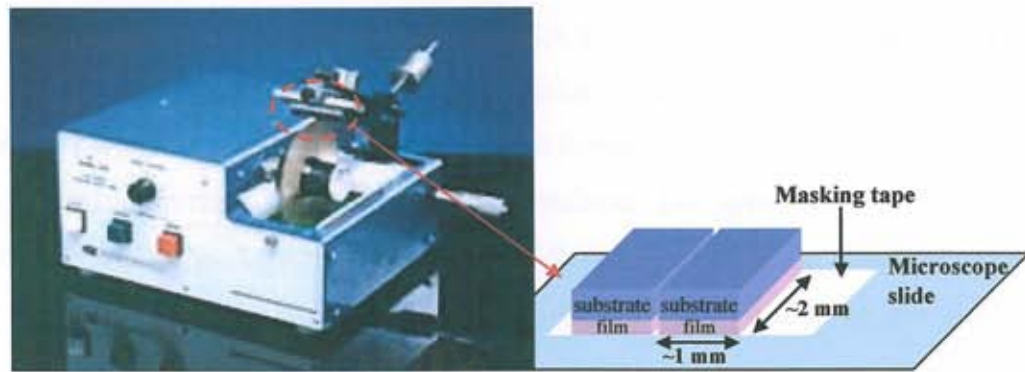
Figure 2.11: Cutting instrument showing a low speed diamond-wheel saw (left) and a cut specimen (right).
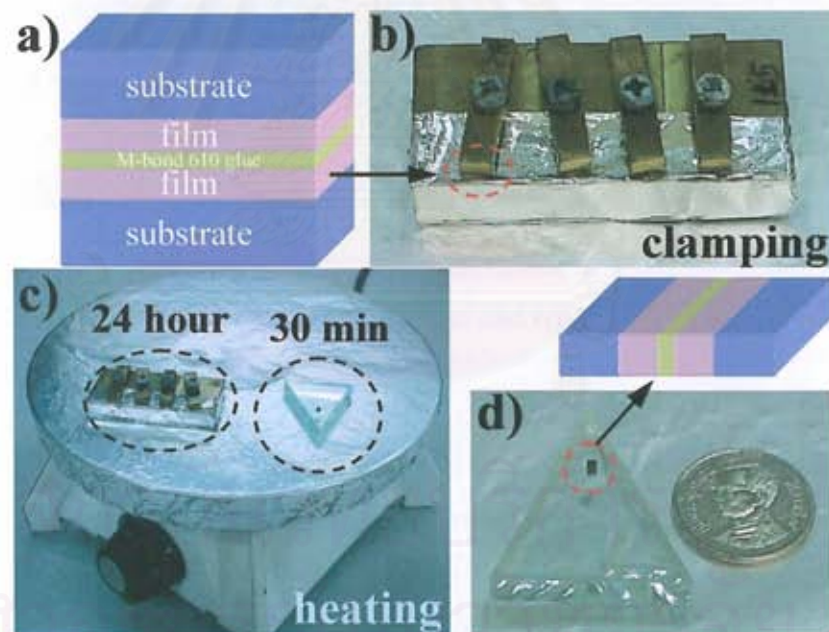
Figure 2.12: (a) Schematic diagram of stuck surfaces of 2 samples. (b) Clamped specimen. (c) Heating clamping holder on the hot plate at 80 °C for 24 hours. (d) Specimen on the triangle shaped glass holder.

Polishing process

The clamped specimen is stuck on the polishing holder (triangular-shaped glass holder) with Kenji glue. This specimen holder is heated on hot plate at 80 °C for 30 minutes which is to dry the glue, as shown Figures 2.12 (c) and (d) . A diamond lapping films is attached on the polishing machine. The specimen is grinded and polished with diamond lapping films that have 9, 6, 3, 1 and 0.5 μm diamond lapping size, respectively, as shown Figure 2.13. To polish the first side of the clamped specimen, the specimen is polished until the thickness is approximately half of its original thickness. Then, the specimen is turned over and polished again until the thickness is approximately about 50 μm.
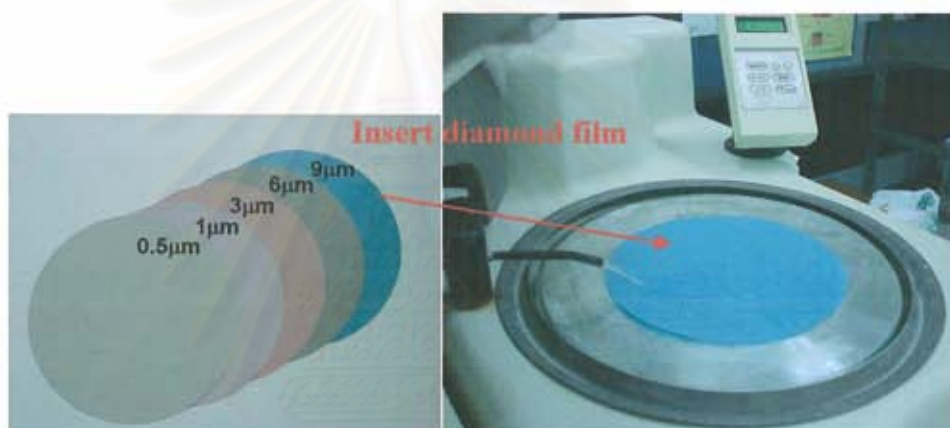
Figure 2.13: (left side) Diamond lapping films and (right side) Diamond lapping film on the polishing machine.

Figure 2.14: (left) Specimen on copper grid and (right) ion beam milling machine.

Ion milling process

A copper grid is stick on the polished specimen with M-BOND 610 glue. Then, the specimen is heated on the hot plate at 80 °C for 4 hours. The specimen on copper grid is taken apart from the polishing holder using acetone. After that, the specimen on copper grid is milled with GATAN Precision Ion Polishing system (PIPs) model 691 (time, voltage and ion beam angle vary depending on the thickness of specimen). Figure 2.14 shows the specimen on copper grid (left) and ion milling machine. In our experiment, Ar^+ ions beam is used with milling conditions as following: milling angle vary from 4° to 10°, 40 keV and milling time about 5 to 10 minutes. The final specimen thickness is almost produced an electron transparency. Lastly, the grid specimen is positioned in TEM system (a JEOL JEM-2010 microscope), which operated at 200 kV.

CHAPTER III
GROWTH INFORMATION AND
INITIAL INVESTIGATIONAL RESULTS

In this chapter, the information of metalorganic vapor phase epitaxial (MOVPE) growth processes and structures of the four types of InGaAs buffer layers used in this study is described. Besides, initial investigational results of all the InGaAs buffer layers, such as composition, surface morphology and strain relaxation, are presented.

3.1 InGaAs Buffer Layers

3.1.1 Growth information

All the $In_xGa_{1-x}As$ buffer layers were grown on (001) GaAs substrates by metalorganic vapor phase epitaxy using trimethylgallium (TMGa), trimethylindium (TMIn) and tertiarybutylarsine (TBAs) as the source materials of Ga, In and As, respectively. The growth was performed at low-pressure of 60 Torr. To prevent the surface roughening of the GaAs substrate, the growth was initially started on the GaAs (001) surface with ~250 nm-thick GaAs buffer layer at 650 °C. Then the temperature was reduced and stabilized at 550 °C for all the growth of InGaAs layers because the In-As bond energy is lower than that of the Ga-As bond and is always kept below 550 °C. For the InGaAs layer, the V/III ([AsH3]/[TMGa]) ratio was fixed to be 15. On the other hand, the ratio of [TMI]/[TMI+TMG] was varied for each sample. The detailed structures of the four types of InGaAs buffer layers are described in the next section.

3.1.2 Structures of samples

In a typical sequence of growth experiments reference samples of InGaAs constant composition layer (CL-InGaAs) would be grown first, followed by a set of samples of InGaAs buffer layers prepared using different growth strategies. Figure 3.1 shows a schematic diagram of the four types InGaAs buffer layers used in this study.

Firstly, Figure 3.1 (a) shows $In_xGa_{1-x}As$ layers with a constant In composition (x) (CL-InGaAs). To calibrate the In concentration, six samples of CL-InGaAs with different ratios of [TMI]/[TMI+TMG] (x_v = 0.1, 0.2, 0.24, 0.3, 0.4 and 0.5) were investigated. Higher incorporation of In is expected due to enrichment of the In supply at higher [TMI]/[TMI+TMG] ratios. Note that, in each sample, the flow supplies of precursors of As and Ga were kept constant. In concentration in the CL-InGaAs layers were examined by high resolution X-ray diffraction (see in Section 3.2.1)

Secondly, Figure 3.1 (b) shows $In_xGa_{1-x}As$ buffer layer on linearly-graded $In_xGa_{1-x}As$ layers (LG-InGaAs). This structure obtained by linear grading the In content of the $In_xGa_{1-x}As$ layer from zero up to some final composition x_f = 0.24, followed by 800-nm-thick $In_{0.24}Ga_{0.76}As$ buffer layer. The grading rate was estimated using the growth conditions of CL-InGaAs to be about 1% In / 40 nm.

Thirdly, Figure 3.1 (c) shows $In_xGa_{1-x}As$ buffer layer on step-graded $In_xGa_{1-x}As$ layers (SG-InGaAs) prepared using 3-step graded type of structure. The two $In_xGa_{1-x}As$ CLs exhibit In concentration of x = 0.8 and 0.16 and thickness of 200 nm, respectively. The top of the graded part consists of a 400-nm-thick $In_{0.24}Ga_{0.76}As$ cap layer with fixed composition x_f = 0.24. The grading rate of the linear grading parts was also estimated using the growth conditions of CL-InGaAs to be about 1% In/ 40 nm.

Lastly, as shown in Figure 3.1 (d), structure of $In_xGa_{1-x}As$ buffer layer on $In_{2x}Ga_{1-2x}As$ /GaAs strained-layer superlattice (SLS) consists of a 60-periods $In_{0.48}Ga_{0.52}As$/GaAs strain-layers superlattice deposited on the top of a 400-nm-thick GaAs buffer layer, and capped by a 400-nm-thick CL-$In_{0.24}Ga_{0.76}As$ as the buffer layer. Thickness and composition of the sample were estimated using the growth conditions of CL-InGaAs.
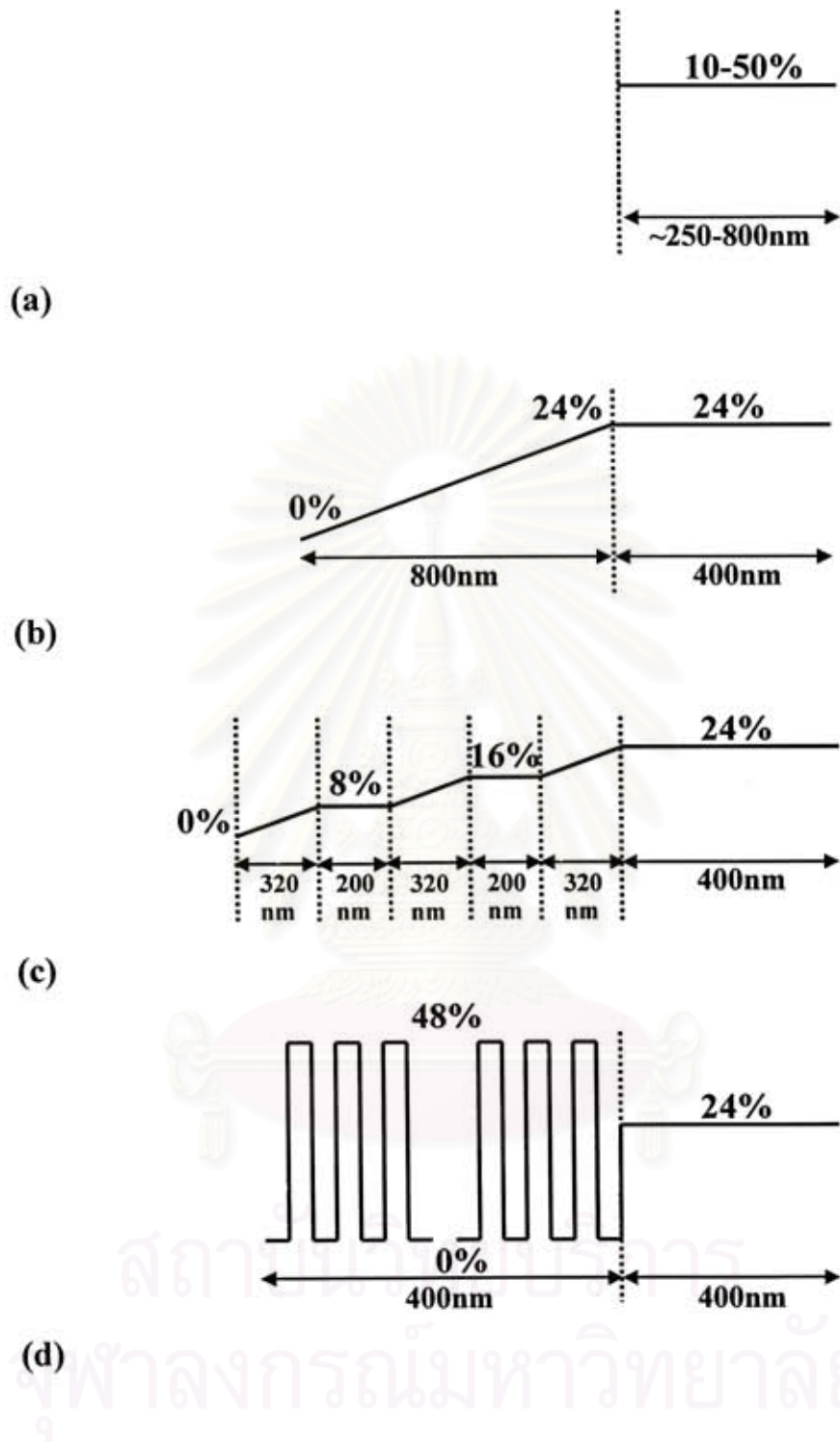
Figure 3.1: Schematic diagram of (a) $In_xGa_{1-x}As$ (x = 0.1, 0.2, 0.24, 0.3, 0.4 and 0.5) constant composition layers, (b) $In_{0.24}Ga_{0.76}As$ buffer layer on linearly-graded $In_xGa_{1-x}As$ layer, (c) $In_{0.24}Ga_{0.76}As$ buffer layer on step-graded $In_xGa_{1-x}As$ layer, and (d) $In_{0.24}Ga_{0.76}As$ buffer layer on $In_{0.48}Ga_{0.52}As$/GaAs strain-layer superlattice.

3.2 Initial Investigational Results

3.2.1 Structural and Compositional investigation

To examine In concentration, HRXRD was carried out. Both (004) symmetric $2\theta/\omega$-scan and (115) asymmetric $\omega-2\theta$ reciprocal space maps were done. Figure 3.2 shows HRXRD (004) profiles of InGaAs layers with different In supplies. With increasing In supply from 10% to 50%, diffraction peak corresponding to InGaAs shift away from the GaAs (004) diffraction peak, as expected from an increasing the lattice-mismatched with raising incorporation of In. Full width at half maximum (FWHM) of diffraction peak corresponding to the InGaAs are increased when In
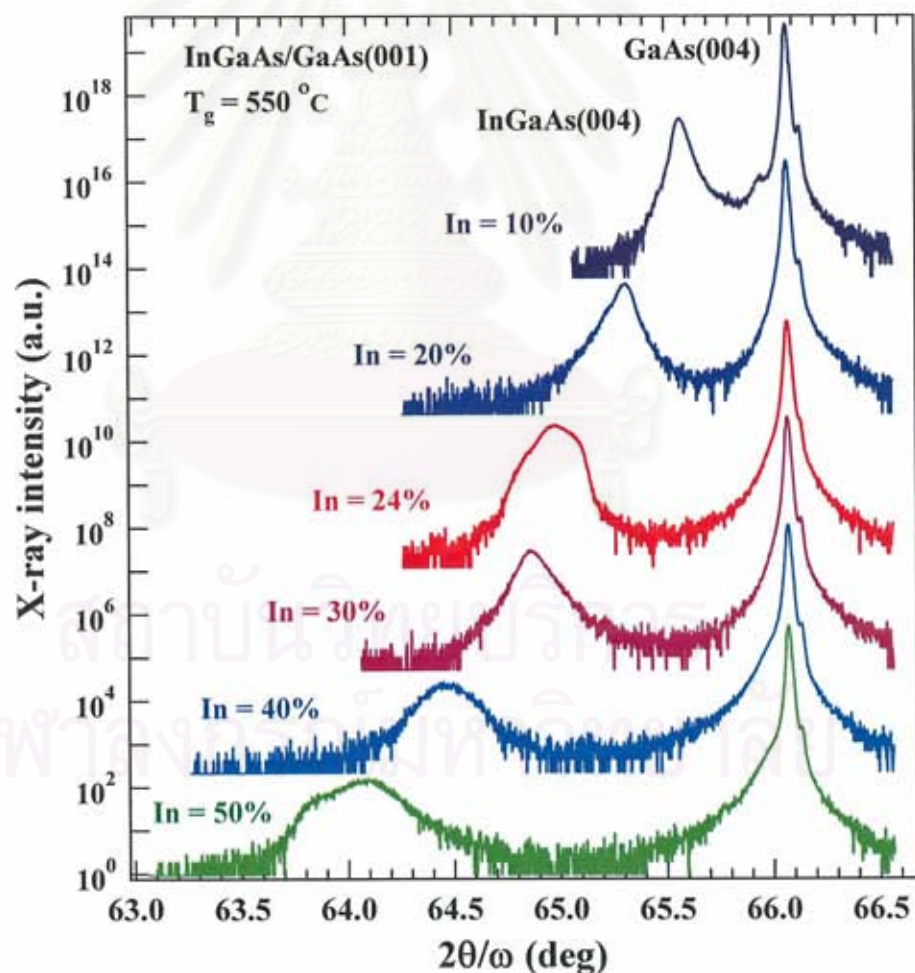
Figure 3.2: High resolution X-ray diffraction (004) profiles of InGaAs layers grown under different In supplies.

supply was increased. This indicates that crystal quality of the InGaAs layers was degraded, resulting in introduction of structural defects into the layer. The perpendicular lattice constant ($a_\perp$), the in-plane lattice constant ($a_{//}$), relaxed lattice constant (a_0), the in-plane lattice mismatch ($f_{//}$), the elastic stiffness constant, (C_{11}, C_{12}) in unit of 10^{11} dyn/cm^2 and the In concentrations (x), which were obtained by HRXRD measurements, are summarized in the Table 3.1. These results demonstrate that, the In concentration (x) differ from the In flow supply (x_v) as following relation, $x_v = 0.68x$. The lattice parameters are raised follow upon In incorporation and are larger than that of GaAs ($a_{GaAs} = 5.653$ Å).

The In concentration in the InGaAs buffer layers on LG-InGaAs, SG-InGaAs and SLS-InGaAs/GaAs were also examined by HRXRD measurements. Figure 3.3 (a) shows HRXRD (004) profile of InGaAs buffer layer on LG-InGaAs. Well-resolved InGaAs (004) diffraction peaks were clearly observed together with the GaAs (004) diffraction peak. We found additional peak near the GaAs diffraction peak assuming that constant layer are generated at the initial stage of the growth. Another peak located at the lowest diffraction angle refers to the InGaAs buffer layer.

In flow supply (%)	$a_\perp$ (Å)	$a_{//}$ (Å)	a_0 (Å)	$f_{//}$ (%)	C_{11}	C_{12}	In concentration in (%)
10	5.692	5.657	5.675	0.07	11.67	5.33	5.5
20	5.713	5.677	5.696	0.43	11.48	5.28	11
24	5.737	5.705	5.722	0.92	11.24	5.22	17
30	5.748	5.719	5.734	1.17	11.13	5.20	20
40	5.780	5.747	5.764	1.66	10.85	5.13	27
50	5.808	5.761	5.785	1.91	10.66	5.09	33

Table 3.1: Summarized of results obtained by HRXRD for all the CL-In$_x$Ga$_{1-x}$As buffer layers. The results show the perpendicular lattice constant ($a_\perp$), the parallel lattice constant ($a_{//}$), lattice constant of relax layer (a_0), the in-plane lattice mismatch ($f_{//}$), the elastic stiffness constant, (C_{11}, C_{12}) in unit of 10^{11} dyn/cm^2 and In concentration.
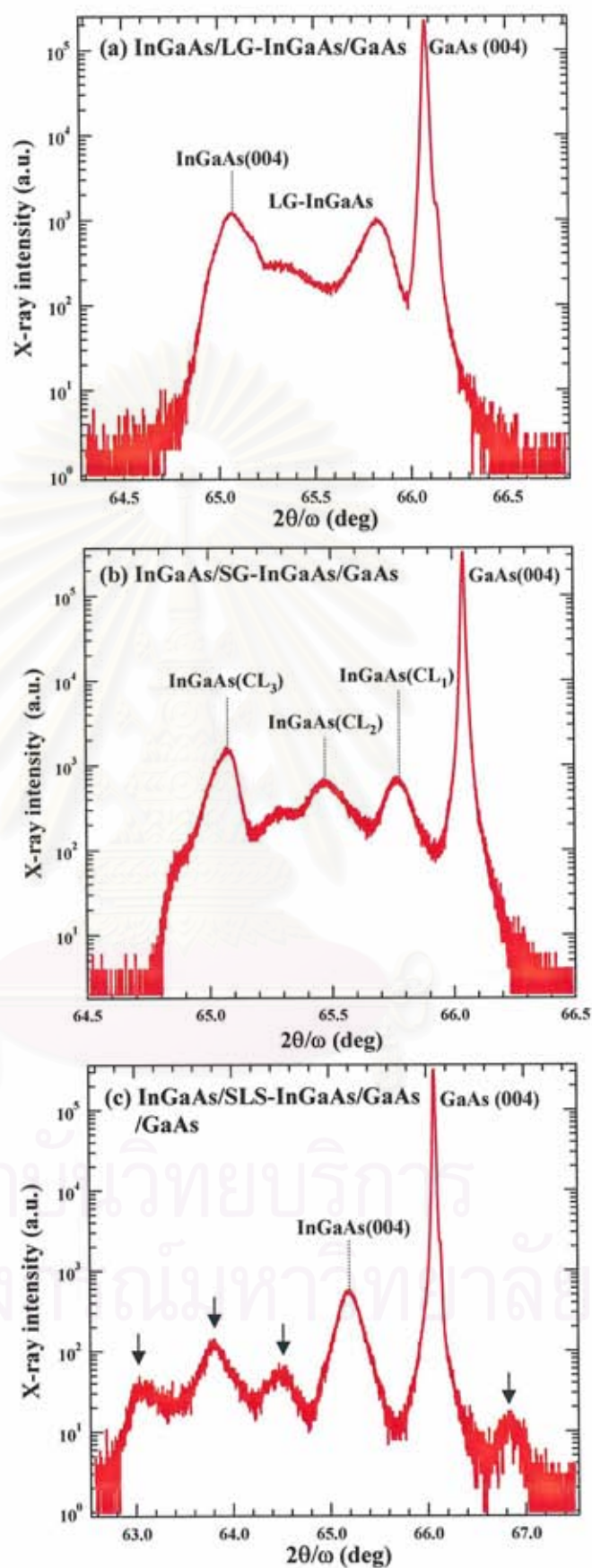
Figure 3.3: High resolution X-ray diffraction (004) profiles of InGaAs buffer layers on (a) LG-InGaAs, (b) SG-InGaAs and (c) SLS-InGaAs/GaAs.

In Figure 3.3 (b), HRXRD (004) profile of the InGaAs buffer layer on SG-InGaAs is shown. It is found that HRXRD pattern consists of broaden curve and well defined diffraction peaks, which are attributed to three CL-layers inserting between the graded parts. Figure 3.3 (c) shows HRXRD (004) profile of the InGaAs buffer layer on SLS-InGaAs/GaAs on GaAs substrate. The arrows indicate the fringes of the interference from the InGaAs/GaAs heteroepitaxial interfaces. This indicates that the SLS-InGaAs/GaAs was successfully grown. The In concentration in all the InGaAs buffer layers were examined using both (004) symmetric $2\theta/\omega$ X-ray diffraction scan and (115) asymmetric $\omega - 2\theta$ reciprocal space maps, as described in Chapter 2. To calibrate the In concentration, thickness and the grading rate in the grading part of the buffer layers, the growth conditions, such as In supply and growth time, were used. It is found that the grading rate of the LG-InGaAs and the SG-InGaAs were 1% In/ 60 nm and 1% In/ 85 nm, respectively. On the other hand, the In concentration and the period-thickness in the superlattice part of the SLS-InGaAs/GaAs is determined to be 33% In and is 17 nm/period, respectively. Structural investigational results of all the InGaAs buffer layers investigated by HRXRD are summarized in Table 3.2. It can be seen that residual strain in all the InGaAs buffer layers are almost relaxed. However, based on data of HRXRD measurements, the value of a_0 and $a_{//}$ is still smaller than that of $a_\perp$. This indicates that all the InGaAs buffer layers are still under compressive-strain. It is evident from HRXRD reciprocal space mapping measurements that the InGaAs buffer layer are partially strain-relaxed from the GaAs substrate. Further, it is found that there is a different of the structural quality between the $In_{0.19}Ga_{0.81}As$ buffer layer on LG-InGaAs, $In_{0.16}Ga_{0.84}As$ buffer layer on SG-InGaAs and $In_{0.17}Ga_{0.83}As$ buffer layer on SLS- $In_{0.33}Ga_{0.67}As$/GaAs from appoint of the values of FWHM for the InGaAs (004) diffraction peaks. FWHM of the InGaAs buffer layers on LG-InGaAs, SG-InGaAs and SLS-InGaAs/GaAs are 9.6, 7.8 and 12.6 min, respectively. This implies that the $In_{0.16}Ga_{0.84}As$ buffer layer on SG-InGaAs layer has higher structural quality than that of the $In_{0.19}Ga_{0.81}As$ buffer layer on LG-InGaAs layer and the $In_{0.17}Ga_{0.83}As$ buffer layer on SLS-$In_{0.33}Ga_{0.67}As$/GaAs.

In$_x$Ga$_{1-x}$As buffer layer on	x (%)	$a_\perp$ (Å)	$a_{//}$ (Å)	a_0 (Å)	$f_{//}$ (%)	FWHM (arcmin)	Thickness* (μm)
LG-InGaAs	19	5.731	5.727	5.730	1.3	9.6	0.95
SG-InGaAs(CL$_1$)	5	5.674	5.671	5.673	0.4	6.1	0.36
SG-InGaAs(CL$_2$)	10	5.697	5.691	5.694	0.7	7.5	0.37
SG-InGaAs(CL$_3$)	16	5.727	5.711	5.720	1.0	7.8	0.95
SLS-InGaAs/GaAs	17	5.721	5.720	5.720	1.2	12.6	0.88

* Layer thicknesses were determined using TEM

Table 3.2: Structural investigational results of the In$_x$Ga$_{1-x}$As buffer layers on LG-InGaAs, SG-InGaAs and SLS-InGaAs/GaAs showing In concentration (x), perpendicular ($a_\perp$), in-plane ($a_{//}$) and relaxed (a_0) lattice constants as well as the in-plane lattice mismatch ($f_{//}$, $\Delta a_{//}/a_s$).

3.2.2 Surface morphologies

In order to study effect of In incorporation on surface morphology of the InGaAs buffer layers, atomic force microscopy (AFM) technique is carried out. Figure 3.3 (a)-(e) shows the surface morphology of the In$_x$Ga$_{1-x}$As layers with constant In concentration of x = 0.055, 0.11, 0.17, 0.20, 0.27 and 0.33, respectively. Figure 3.3 (a) appears as a network of crossing lines in directions of [110] and [1-10]. It is clearly seen that such crossing lines become denser due to an increasing In concentration as shown in Figure 3.3 (b)-(d). Since, the MOVPE grown epitaxial films, which are not lattice-match to underlying substrates, generally exhibits crossing lines surface known as "cross-hatch pattern" [36]. Cross-hatch pattern was first reported by Burmeister [37] in the GaAsP/GaAs heterostructure and also investigated in other lattice-mismatched systems such as GaAs/Si [38] and InGaAs/InP [39]. Figure 3.3 (a)-(d) exhibits cross-hatch morphology in the feature of two-dimensional (2D) growth mode (layer-by-layer) which has In content below 0.2 (x<0.2). We believe this feature related to the generation of interfacial MDs, resulting in the relaxation of the residual strain and two-dimensional (2D) growth [40]. AFM image, in Figure 3.3 (e), shows an appearance of the transition of the 2D growth mode to the three-dimensional (3D) growth mode. On the other hand, Tamura *et al.* have
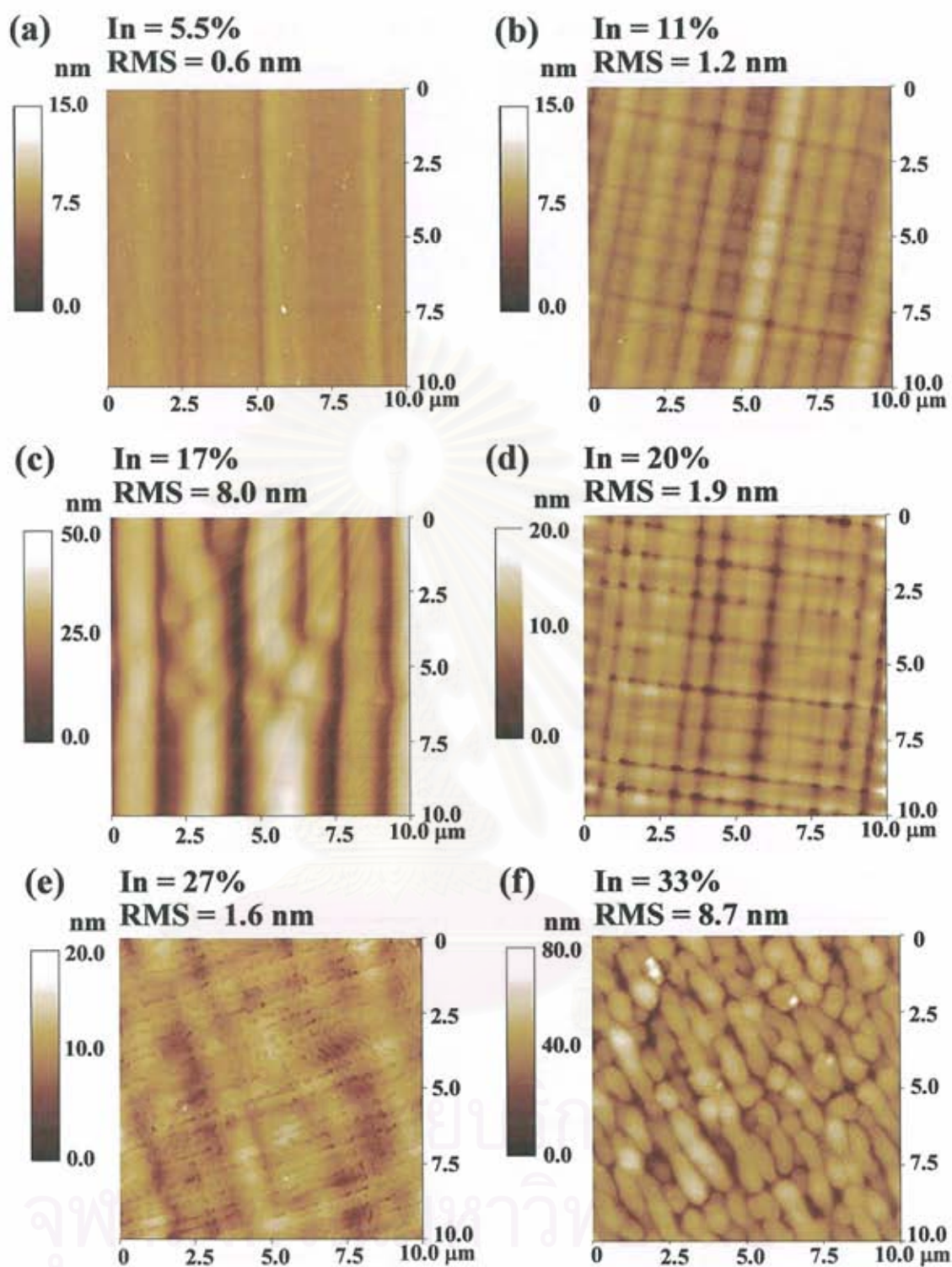
Figure 3.4: AFM images of $In_xGa_{1-x}As$ layers with different In concentrations (a) $In_{0.05}Ga_{0.95}As$, (b) $In_{0.11}Ga_{0.89}As$, (c) $In_{0.17}Ga_{0.93}As$, (d) $In_{0.20}Ga_{0.80}As$, (e) $In_{0.27}Ga_{0.73}As$ and (f) $In_{0.33}Ga_{0.67}As$.
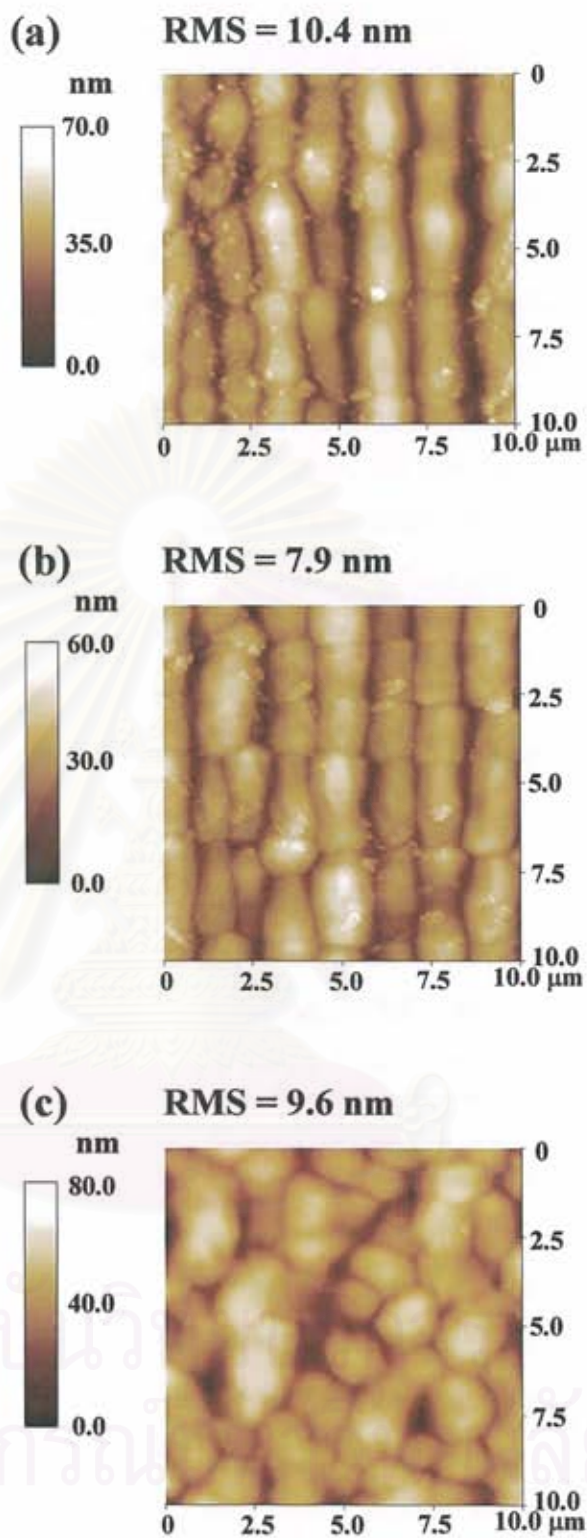
Figure 3.5: AFM images of (a) $In_{0.19}Ga_{0.81}As$ buffer layer on LG-InGaAs, (b) $In_{0.16}Ga_{0.84}As$ buffer layer on SG-InGaAs and (c) $In_{0.17}Ga_{0.83}As$ buffer layer on SLS-InGaAs/GaAs.

reported that, for $x \leq 0.2$, the 2D layer-by-layer growth is operative, while for $x \geq 0.3$, the 3D island growth mode is dominated. For $0.2 < x < 0.3$, the growth mode should be the intermediate stage from the 2D growth mode transition to the 3D growth mode. Our results are corresponding to the results reported by Tamura *et al*. It was suggests that an increasing In concentration strongly affects on the surface morphology and generation of misfit dislocation at interface due to higher lattice-mismatching.

Next, we also examined the effect of LG-InGaAs, SG-InGaAs and SLS-InGaAs on the surface morphology of the InGaAs buffer layer, as shown in Figure 3.4. It is seen that, for the InGaAs buffer layers on LG- and SG-InGaAs, the surface morphology still exhibits cross-hatch like-pattern, indicating domination of 2D growth mode (Figure 3.4 (a) and (b)). The 3D island growth mode was exhibited in the $In_{0.17}Ga_{0.83}As$ buffer layer on SLS-InGaAs/GaAs (Figure 3.4 (c)).

3.3 Strain Relaxation in InGaAs Buffer Layers

In this part, initial investigated results of strain properties in InGaAs buffer layers, such as residual strain ($\varepsilon_{//}$) and strain factor (*f*), are discussed. Figure 3.6 summaries the measured (a) residual strain and (b) strain factor of the $In_xGa_{1-x}As$ layers on GaAs substrates with In content of 5.5-33%. It is seen that the values of residual strain in all the layers are about 0.25-0.45%, indicating an appearance of strain relaxation in the layers. However, note that the values of residual strain in all the InGaAs layers are almost the same value. On the other hand, as seen in Figure 3.6 (b), the values of strain factor, which reflect to the strain relaxation in the layers, is decreased from 80% to 20% for the InGaAs layers with In concentrations of 5.5% and 33%, respectively. A large reduction of the strain factor is due to the strain relaxation of the lattice by an introduction of MDs. These results suggest that all the InGaAs layers are under partially strained.

Now we return the discussion of the analysis of the asymmetric (115) HRXRD $\Delta 2\theta / \omega - \Delta \omega$ mapping. For comparison, the (115) HRXRD maps of the four different InGaAs buffer layer grown using different strategies are shown in Figure 3.7. As shown in Figure 3.7, no rotation of the elliptic contour, which indicates an existence of the residual strain in the layer, were observed. It is clear from Figure 3.7 (b)-(d) that both ω-mode and $2\theta / \omega$-mode FWHM from InGaAs buffer layers on LG-, SG- and SLS-InGaAs are broaden compared to those from InGaAs layer on

(a) **(b)**
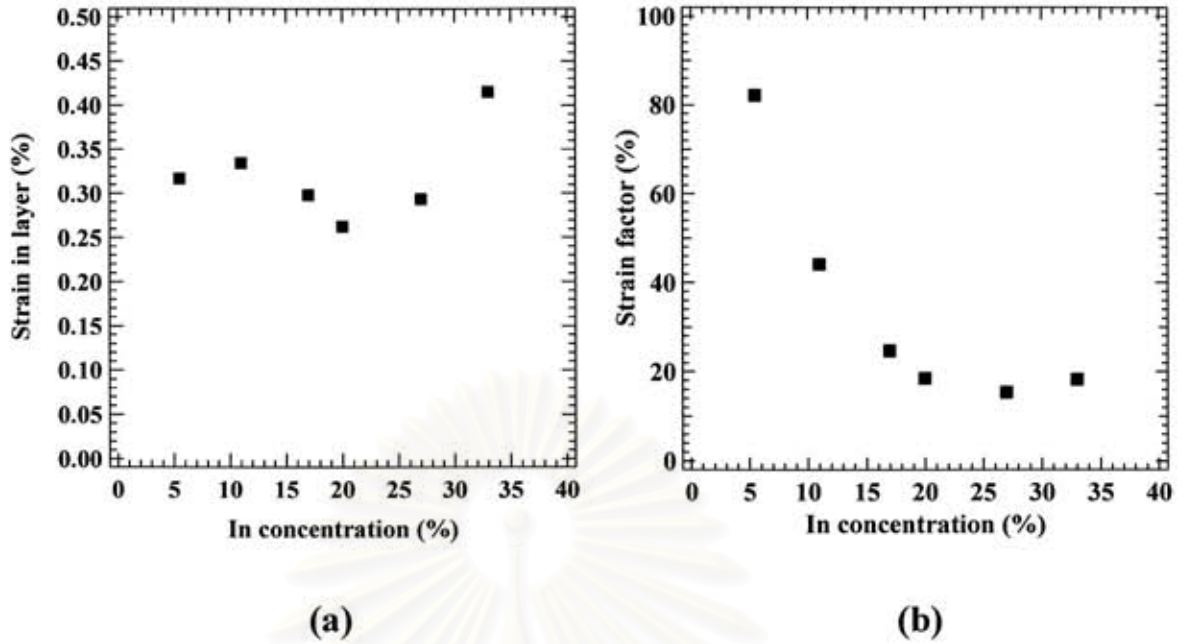
Figure 3.6: Calculated values of (a) residual strain (%) and (b) strain factor (%) of In$_x$Ga$_{1-x}$As layers with different In concentrations of x = 5.5, 10, 17, 20, 27 and 33%.

GaAs (Figure 3.7 (a)). This means that the crystal mosaicity and the lattice-relaxation in InGaAs on LG-, SG- and SLS-InGaAs are larger than those in InGaAs on GaAs. On the other hand, the broadening in ω-mode FWHM from the InGaAs buffer layers on LG-, SG- and SLS-InGaAs (Figure 3.7 (b)-(d)) is apparently limited by the mosaic of the graded and superlattice patrs. Since the mosaicity in the LG-, SG- and SLS-InGaAs parts is larger than that of the GaAs substrate, the mosaicity of InGaAs buffer layers grown on the LG-, SG- and SLS-InGaAs should be also large. However, it is considered to be not sufficient to dominate the buffer layer properties. Table 3.3 summarizes the measured lattice parameters of the InGaAs buffer layers perpendicular ($a_\perp$) and parallel ($a_{//}$) to the GaAs (001) surface and in-plane lattice-mismatch ($\varepsilon_{//} = \Delta a_{//} / a$), strain factor and FWHM of asymmetric (115) $\Delta\omega$. The measured lattice paramenters for InGaAs show that substantial tensile strain along [001] direction is present in the InGaAs buffer layers on SG-InGaAs and GaAs. This tensile strain is attributable to an imperfect lattice relaxation at the heteroepitaxial interface. On the other hand, fully relaxed layers with the smallest value of residual strain were clearly observed for the InGaAs buffer layers on SLS-InGaAs and LG-InGaAs.
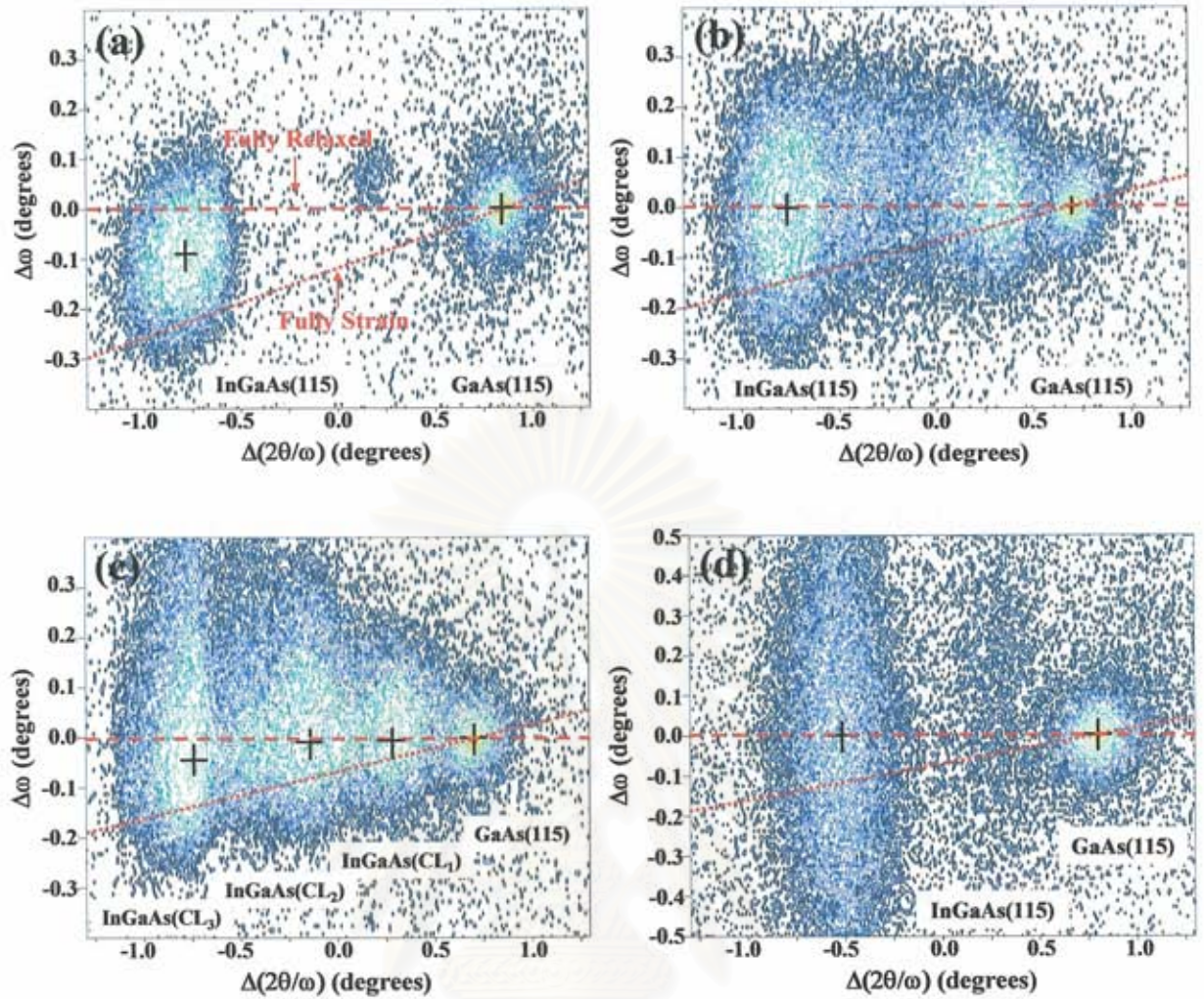
Figure 3.7: Asymmetric (115) HRXRD maps of (a) $In_{0.17}Ga_{0.83}As$ on GaAs, (b) $In_{0.19}Ga_{0.81}As$ on LG-InGaAs, (c) $In_{0.16}Ga_{0.84}As$ on SG-InGaAs and (d) $In_{0.17}Ga_{0.83}As$ on SLS-InGaAs/GaAs.

$In_xGa_{1-x}As$ buffer layer on	x (%)	$a_\perp$ (Å)	$a_{//}$ (Å)	a_0 (Å)	$f_{//}$ (%)	$\varepsilon_{//}$ (%)	Strain factor (%)	FWHM ($\Delta\omega$)
GaAs	17	5.737	5.705	5.722	0.9	0.30	25	0.16
LG-InGaAs	19	5.731	5.727	5.730	1.3	0.05	4.0	0.20
SG-InGaAs	16	5.727	5.711	5.720	1.0	0.16	13	0.17
SLS-InGaAs/GaAs	17	5.721	5.720	5.720	1.2	0.01	0.1	0.33

Table 3.3: Lattice parameters ($a_\perp$, $a_{//}$ and a_o), lattice misfit (f), residual strain ($\varepsilon_{//}$), strain factor and FWHM of asymmetric (115) for the $In_xGa_{1-x}As$ buffer layers on GaAs, LG-InGaAs, SG-InGaAs and SLS-InGaAs/GaAs.

3.4 Summary

The InGaAs buffer layers on GaAs, LG-InGaAs, SG-InGaAs and SLS-InGaAs/GaAs grown by MOVPE were initially investigated. First, it is found that higher incorporation of In directly effects on the strain properties of the $In_xGa_{1-x}As$ layers on GaAs substrates, as follows.

(1) Increase of lattice-mismatching between the InGaAs layer and the GaAs substrate

(2) Reduction of residual strain and strain factor

(3) The cross-hatch morphologies, resulting from the generation of misfit dislocations at interface owing to 2D growth mode, for In concentration lower than 20%

(4) Growth mode transition from the 2D growth mode to the 3D island growth mode for the In concentration higher than 30%

On the other hand, it is found that the InGaAs buffer layers on GaAs, LG-InGaAs, SG-InGaAs and SLS-InGaAs/GaAs are mostly relaxed from the GaAs substrate. The observation of strain relaxation in InGaAs buffer layers are arrange from SLS-InGaAs, LG-InGaAs, SG-InGaAs and CL-InGaAs, respectively. The surface morphology exhibits 2D growth mode in LG-InGaAs and SG-InGaAs and shows 3D growth mode in SLS-InGaAs/GaAs.

CHAPTER IV
TEM INVESTIGATION OF InGaAs
BUFFER LAYERS

In this chapter, we describe the investigational results of the InGaAs buffer layer grown on GaAs, LG-InGaAs, SG-InGaAs and SLS-InGsAs/GaAs using transmission electron microscopy. The main type of structural defects in the InGaAs buffer layers is found to be a linear defect (dislocations). Based on TEM data, we clarify the dislocation types, which are strongly depended on the epitaxial growth as well as the material properties of epitaxial layer, such as lattice parameter, thermal expansion coefficient, and bond strength, etc. Accordingly, simple models are also used to describe the formation mechanism of such dislocations in microscopic scale. Finally, a comparison of microstructural properties between the four types of InGaAs buffer layer is discussed.

4.1 Microstructures of InGaAs on GaAs
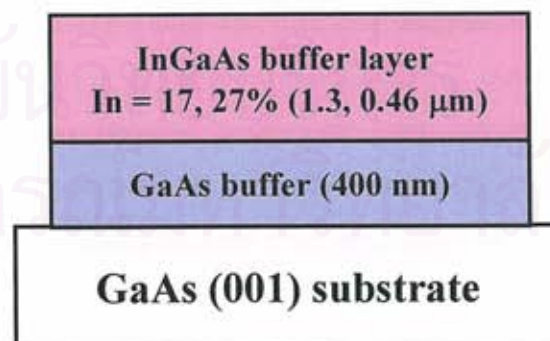
Figure 4.1: Schematic illustration of the $In_{0.17}Ga_{0.83}As$ and $In_{0.27}Ga_{0.73}As$ layers grown on GaAs (001) substrates. Layer thicknesses of the $In_{0.17}Ga_{0.83}As$ and $In_{0.27}Ga_{0.73}As$ layers are 1.3 and 0.46, respectively.
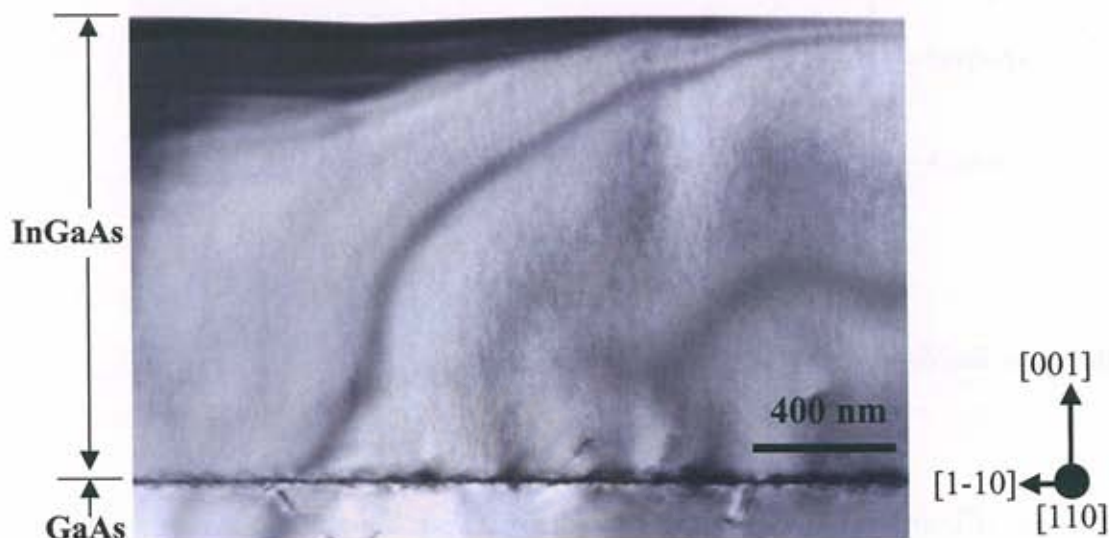
Figure 4.2: Bright-field TEM image of In$_{0.17}$Ga$_{0.83}$As buffer layer on GaAs.

In this part, the In$_{0.17}$Ga$_{0.83}$As and In$_{0.27}$Ga$_{0.73}$As layers, on GaAs (001) substrates with different In concentrations and thickness but similar residual strain ($\varepsilon_{//}$ = 0.3%) were selected to investigate the dislocation mechanism. Figure 4.1 shows a schematic illustration of the In$_x$Ga$_{1-x}$As buffer layer with In concentrations and thickness of 17% and 27% and 1.3 µm and 0.46 µm, respectively. To understand dislocation mechanism in InGaAs on GaAs, the In$_{0.17}$Ga$_{0.83}$As and In$_{0.27}$Ga$_{0.73}$As layers were investigated by cross-section TEM. The bright-field TEM micrograph shown in Figure 4.2 represents the In$_{0.17}$Ga$_{0.83}$As layer on GaAs. It is clearly seen that the MDs visible by their strain contrast, are located near the InGaAs/GaAs heteroepitaxial interface. This dominant is seen as black-doted contrasts at interface. Above-mentioned in heteroepitaxy found that it is very difficult to grow crystal with low density of dislocations owing to creation of dislocations during the growth and subsequent cooling down. Formation of black-doted contrasts demonstrates that an interface with lattice misfit is formed between the epitaxial layer and the substrate. Three types of interface are possible, namely coherent, semi-coherent and incoherent interfaces. Coherent interface occurs when the lattice parameters of the epitaxial layer and the substrate have perfect lattice-matching. Semi-coherent interface between the epitaxial layer and the substrate in which there is partial lattice-matching. As shown in Figure 4.3, the boundary of partial lattice-matching interface is separated by regions of distortion, i.e. dislocations. Finally, incoherent interface appears when there is no lattice matching as grain boundary.
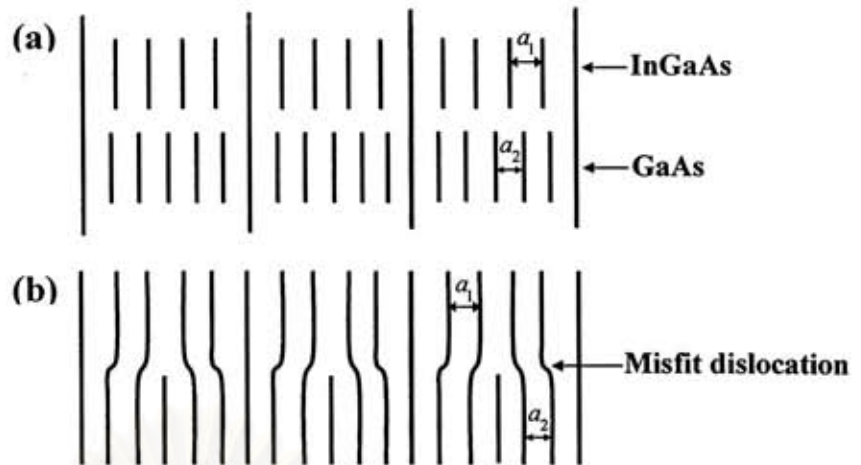
Figure 4.3: Coincidence model of an interface with lattice misfit; (a) perfect coincidence lattice with a lattice plane ratio of m/n = 5/6, (b) coincidence lattice with coherence relaxation within the unit cells. a_1 and a_2 show lattice constant of InGaAs and GaAs, respectively.

From the three types of interface described above, the semi-coherent interface is possible considered in the case of the InGaAs/GaAs interface corresponding to the coincidence models of an interface with lattice misfit, as shown in Figure 4.3 [41]. For example, the perfect coincidence lattice with a lattice plane (m) of InGaAs is m = 5 and a lattice plane (n) of GaAs is n = 6. This indicates that the lattice constant of InGaAs is larger than GaAs (Figure 4.3 (a)) and, then, the accommodations of lattice planes at the interface are shown in Figure 4.3 (b). The boundary between the InGaAs layer and the GaAs substrate indicated to misfit dislocations as seen in the TEM image (Figure 4.2). Based on the coincidence model, the black-doted contrasts in our TEM image shown in Figure 4.2 are analyzed to be MDs, which is due to the lattice-mismatching occurred during the epitaxial growth. In the TEM image, different size of black-doted contrasts is due to the generation of dislocation cores and lattice distortion. Consistent with the HRXRD measurements (Section 3.3) and surface morphology (Section 3.2.2) described in the Chapter 3, the generation of misfit dislocations is visible at the InGaAs/GaAs interface. Although, the misfit dislocations do not propagate through the InGaAs layer, we found that the strain contrast, which is attributable to the preparation of very thin specimen, propagates from GaAs to the InGaAs layer.
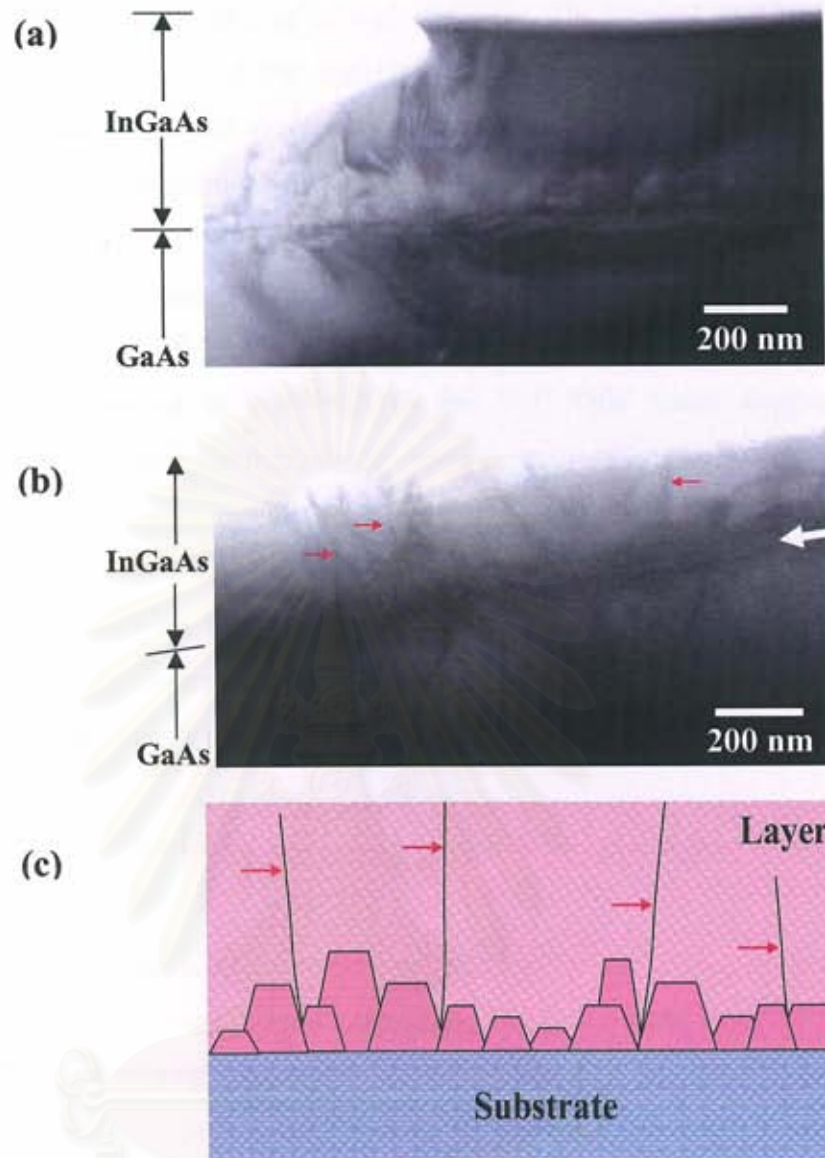
Figure 4.4: Bright-field TEM images of $In_{0.27}Ga_{0.73}As$ buffer layer on GaAs. (b) is a selective area thicker than area (a). (c) shows a schematic diagram of 3D growth mode. Red arrows indicated threading dislocations (TDs) generating at the interface and propagating though the layer.

Next, the $In_{0.27}Ga_{0.73}As$ layer on GaAs is examined to investigate effect of In incorporation on the formation of micro-structural defects. Figure 4.4 (a)-(b) shows cross-section BF-TEM micrographs of $In_{0.27}Ga_{0.73}As$/GaAs with different areas. Also, Figure 4.4 (c) shows a schematic diagram of the 3D island growth mode [18]. It is clearly seen that the misfit dislocations are generated at heteroepitaxial interface. In addition, we find the island-like features near InGaAs interface and line-contrasts,

propagating from the interface to through the layer. The line-contrast is obvious seen in thicker selective area of the specimen, as shown in Figure 4.4 (b). Further, according to the island-like surface morphology (see Figure 3.5 (c)), then, we can create a schematic diagram of the growth mode as the 3D island growth mode, as shown in Figure 4.4 (c). We can explain this growth as follows. Coalescence of the islands during the epitaxy has led to the introduction of undesired threading dislocations [42], which transmit through the InGaAs layer up to the free surface. Thus, the line-contrast is attributed to the TD. This result suggests that the introduction of structural defects in the heteroepitaxy is not only dependent on the lattice-mismatch but also strongly affected by the growth mechanism. With increasing In concentration, a higher number of structural defects is present in the layer than that observed in layer with lower In concentration. The introduction of TDs in the heteroepitaxy is the understanding of the actual growth mode during the initial stage of the epitaxial process, especially when the 3D island growth occurs.

4.2 Microstructures of InGaAs on LG-InGaAs

Figure 4.5 shows a schematic illustration of the $In_{0.19}Ga_{0.81}As$ buffer layer on the linearly-graded layer grown on the GaAs (001) substrate in accord with cross-section BF-TEM micrographs shown in Figure 4.6. For the linearly-graded part in Figure 4.6, the dislocations are spread throughout the graded layer, while a
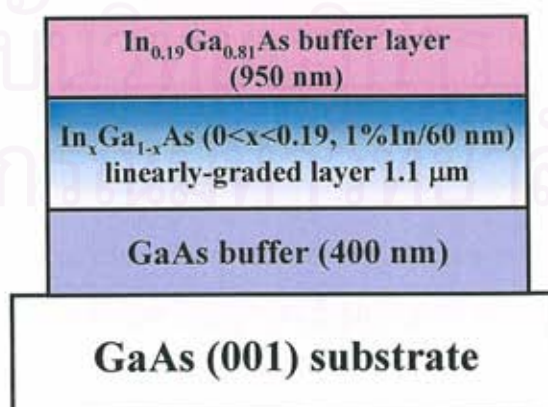
Figure 4.5: Schematic illustration of the $In_{0.19}Ga_{0.81}As$ buffer layer on the linearly-graded InGaAs layer grown on GaAs (001) substrate.
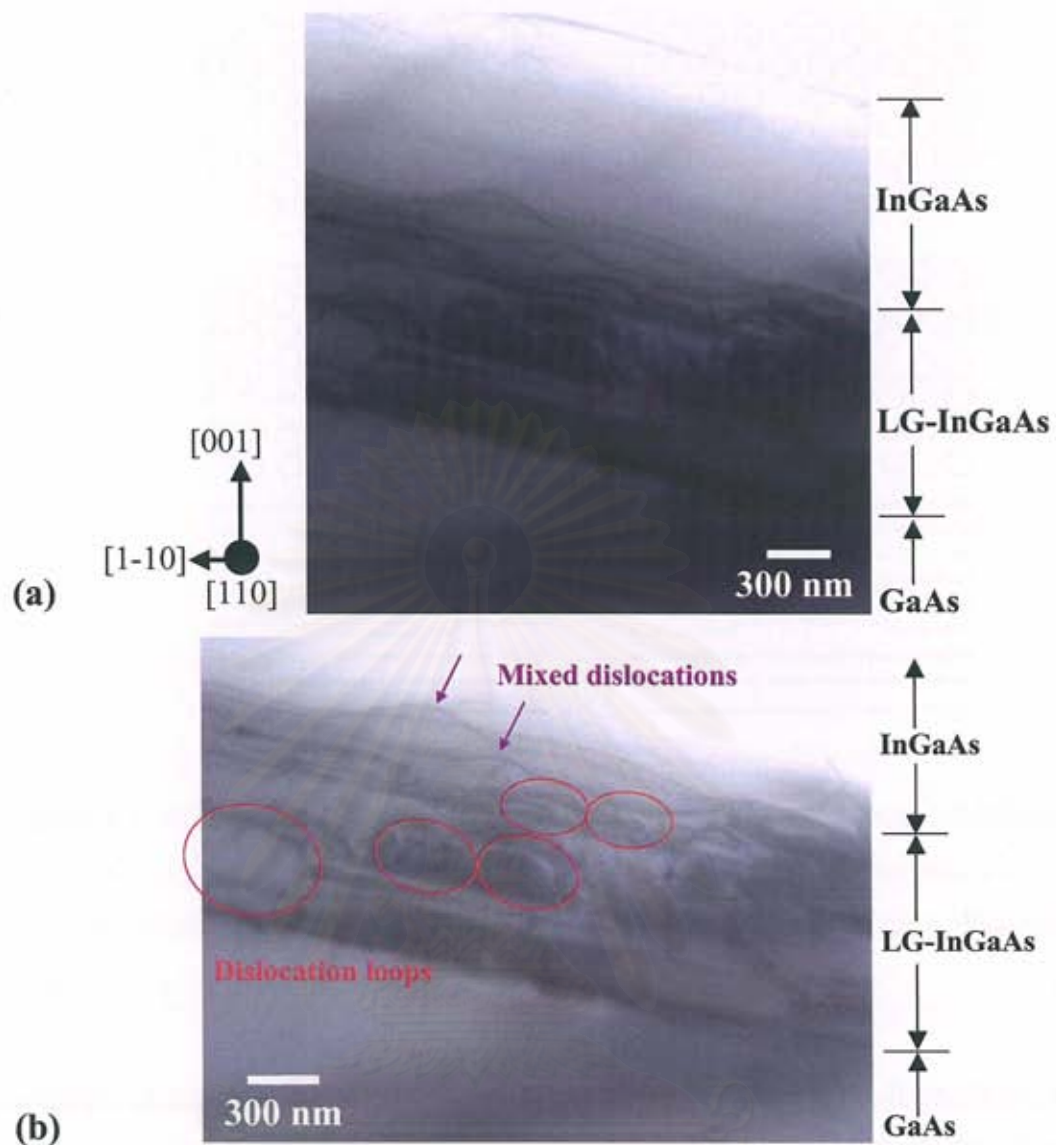
Figure 4.6: Cross-section BF-TEM micrographs showing (a) the linearly-graded structure depicted in Figure 4.5 and (b) the structural defects, which are generated within the linearly graded part. Mixed dislocations and dislocation loops are indicated by violet arrows and red circles, respectively.

dislocation-free layer was observed in the $In_{0.19}Ga_{0.81}As$ buffer layer. This demonstrates that the InGaAs buffer layer with high crystal quality and full relaxation was grown. In general, however, dislocations are bent and irregular, especially after plastic deformation. It is found that the shape of dislocation can be curve line, as shown in Figure 2.3 (c), which is a boundary separating the slipped and unslipped regions of the crystal. This boundary is attributed to mixed-type dislocation which is a transition region between edge and screw dislocations. Therefore, the curvature-line
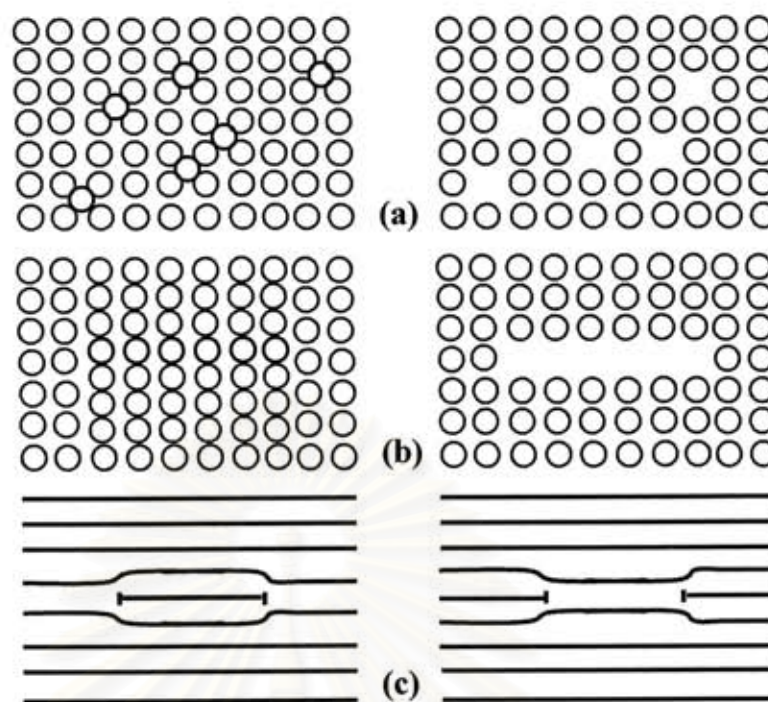
Figure 4.7: Schematic illustration of the formation of dislocation loop. (a) Represents a crystal with a large non-equilibrium concentration of interstitials (left) and vacancies (right). (b) The interstitials and vacancies have complied on a close-packed plane and (c) the habit plane of the dislocation loop.

contrasts in our TEM micrograph are assigned to be mixed-type dislocations while looking along $\langle 001 \rangle$ direction, as shown in Figure 2.3 (c). It is found that the characteristics of loop-line contrasts are half and full loops (Figure 4.6 (b), red circles). In atomic scale, if the dislocation consists of an extra plane of atoms (or a missing plane of atoms) lying entirely within the crystal, then the dislocation is known as a dislocation loop. The dislocation line of the dislocation loop forms a closed curve that is usually circular in shape. The formation of loop-line is generated with a large non equilibrium concentration of vacancies and interstitials [19] and they have complied on a close-packed plane, as shown in Figures 4.6 (a) and (b). The determination of loop-line requires the knowledge of the habit plane of the dislocation loop (Figure 4.7 (c)). The types of dislocation loop depend on character of the habit plane [43]. The vacancy type of the dislocation loop exhibits to missing plane of atoms in the perfect crystal and the interstitial type of the dislocation loop display to extra plane of atom. Results from our TEM micrograph show that the loop-line contrasts are possible

explained as the dislocation loop, which shows both the interstitial and vacancy types. High density of dislocations in the linearly-graded part strongly suggests that the graded layer must achieve full relaxation, which effect to strain relief in the $In_{0.19}Ga_{0.81}As$ buffer layer. However the dislocations density has unequal in the all of linearly-graded layer, it is due to the different degree of relaxation in each region. In this sample the both initial growth and post-growth are examined beside lattice mismatch and growth mechanism (3D) in constant buffer layer to generation of dislocation. Owning to the majority of dislocation lines are generate horizon with interface. It has been supposed that, strain relaxation is occurred during cooling down process, owing to the difference in properties of the epitaxial layer and substarte that are thermal expansion coefficient, elastic stiffness constant and bond strength. The Table 4.1 summarizes values of material properties of GaAs and InAs. Using the linear interpolation of coefficient of thermal expansion and bond strength between InAs and GaAs, when increasing In concentration, the values of coefficient of thermal expansion and bond strength are decreased as well as elastic stiffness constant. The analyzed results suggest that the growth of linearly graded layer can be compared as small step over and over interface. The bond strength of $In_xGa_{1-x}As$ is decrease so the distortion of bond is possible origin of dislocation lines, which are nucleated at small step parallel to interface of graded layer.

Binary compound materials	Thermal expansion coefficient $(\times 10^{-6}/°C)$	Elastic stiffness constant $(10^{11}dyn/cm^2)$	Bond strength at 25 °C (KJ/mol)
In-As	4.52	$C_{11}= 8.329, C_{12}= 4.526$	201
Ga-As	6.86	$C_{11} = 11.88, C_{12}= 5.38$	209.6 ± 1.2

Table 4.1: Thermal expansion coefficient, elastic stiffness constant and bond strength of In-As and Ga-As [33].
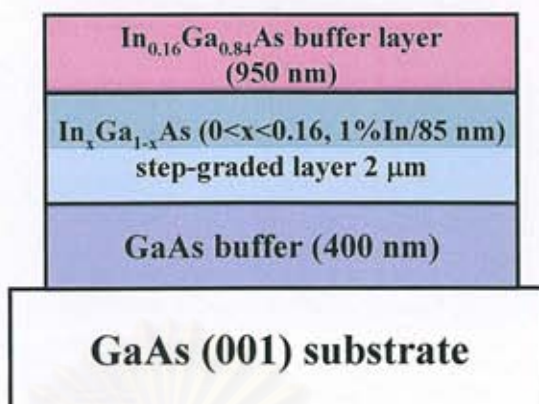
Figure 4.8: Schematic illustration of the $In_{0.16}Ga_{0.84}As$ buffer layer on step-graded layer grown on GaAs (001) substrate.

4.3 Microstructure of InGaAs on SG-InGaAs

Next, we investigate the sample of $In_{0.16}Ga_{0.84}As$ buffer layer on SG-InGaAs grown on GaAs substrate, as shown in Figure 4.8. Sample structure consists of 3-CL-InGaAs and 3-LG-InGaAs layers. In Figure 4.9, cross-sectional BF-TEM micrograph shows that the majority of the misfit dislocations are confined to the LG-InGaAs layers. In addition, the occurrence of threading dislocations is observed in constant layers (pink arrows) which generate from linearly-graded regions. It is clearly seen that the dislocation loops are also visible in LG_3-InGaAs region. The effect of having composition steps and constant composition layers in the structure is to confine the misfit dislocations to the interfacial regions between layers. As described in Chapter 3, the residual strain in $In_{0.05}Ga_{0.95}As$, $In_{0.10}Ga_{0.90}As$ and $In_{0.16}Ga_{0.84}As$ constant layer is 0.03%, 0.05% and 0.16%, respectively, since the distribution of dislocations density in each LG-InGaAs, which is unequal effects to a generation of dislocation in the CL-InGaAs layers. If LG-InGaAs is less relaxed, this demonstrated an existence of residual strain in the CL-InGaAs and LG-InGaAs layers. This is due to the thickness of each LG-InGaAs is not enough to strain relieve, then, the CL-InGaAs layers are also strained. It has been suggest that raising thickness of LG-InGaAs is required in $In_{0.19}Ga_{0.81}As$ buffer layer on SG-InGaAs sample.
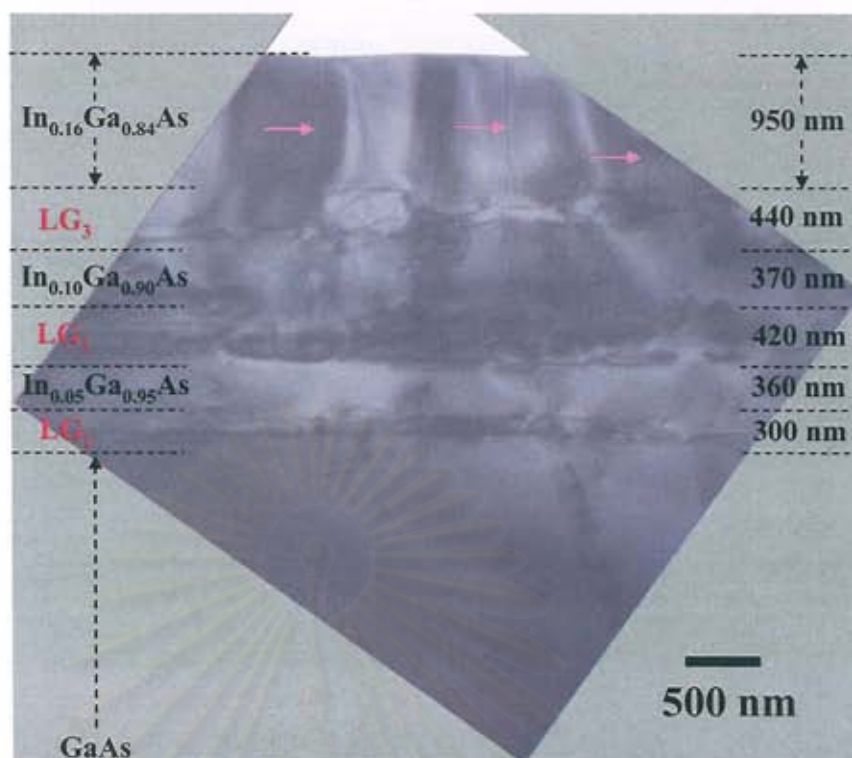
Figure 4.9: Cross-section BF-TEM micrograph showing the $In_{0.16}Ga_{0.84}As$ buffer layer on step-graded structure grown on GaAs substrate.

4.4 Microstructures of InGaAs on SLS-InGaAs/GaAs
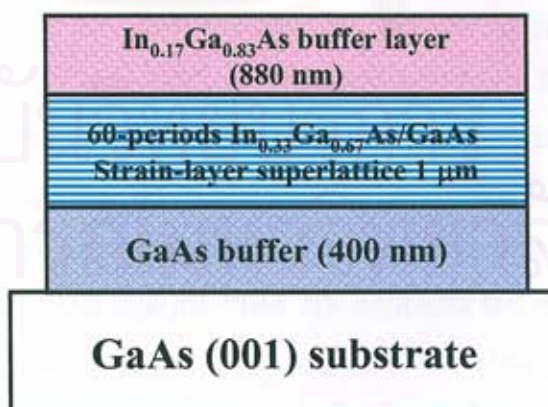
Figure 4.10: Schematic illustration of the $In_{0.17}Ga_{0.83}As$ buffer layer on the strain-layer superlattice InGaAs/GaAs grown on GaAs (001) substrate.
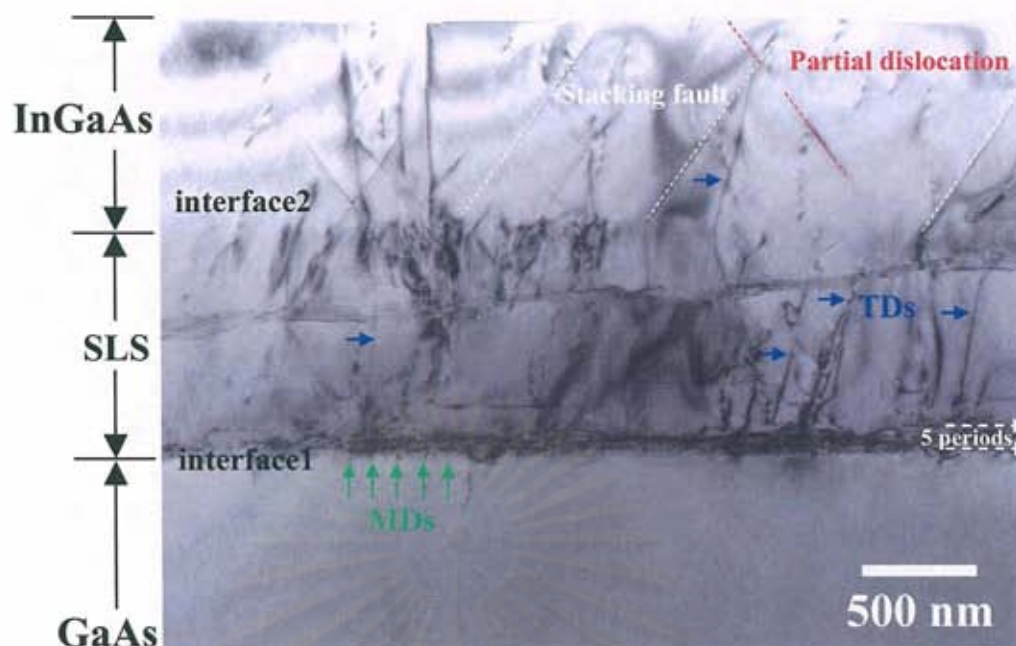
Figure 4.11: Cross-section BF-TEM micrograph showing the $In_{0.17}Ga_{0.83}As$ buffer layer on the strain-layer superlattice InGaAs/GaAs grown on GaAs (001) substrate corresponding to Figure 4.10.

Lastly, the $In_{0.17}Ga_{0.83}As$ buffer layer on strain-layer superlattice InGaAs/GaAs (SLS-$In_{0.33}Ga_{0.67}As$/GaAs) grown on GaAs (001) substrate was investigated and discussed. Figure 4.10 shows a schematic diagram for structure of the $In_{0.17}Ga_{0.83}As$ buffer layer on the SLS-InGaAs/GaAs. Cross-section BF-TEM micrograph is shown in Figure 4.11. Certainly, we see formation of MDs at the interface 1 as an indicated by green arrows. In general, contrasts of threading dislocations in the SLS-$In_{0.33}Ga_{0.67}As$/GaAs are wavy, especially first 5 periods of the superlattice and some part of TDs continuance to surface indicated by blue arrows (Figure 4.11). The cross-section BF-TEM micrograph in the InGaAs buffer layer region shows distinct tilted line contrasts which are inclined at about 54.7° to the GaAs (001) surface. This mean that the tilted line contrasts are nearly parallel to the {111} planes in the InGaAs buffer layer throughout to surface (white line, Figure 4.11). This tilted line contrasts are known as dominant feature of stacking faults generating in the cubic symmetry. Stacking fault generated along the cubic (111) plane is an insertion of 1 monolayer of hexagonal structure between two single crystalline cubic structures rotated by 60° [44]. Moreover we can be seen some tilted line contrasts end inside buffer layer and beginning again in crystal. Figure 4.12
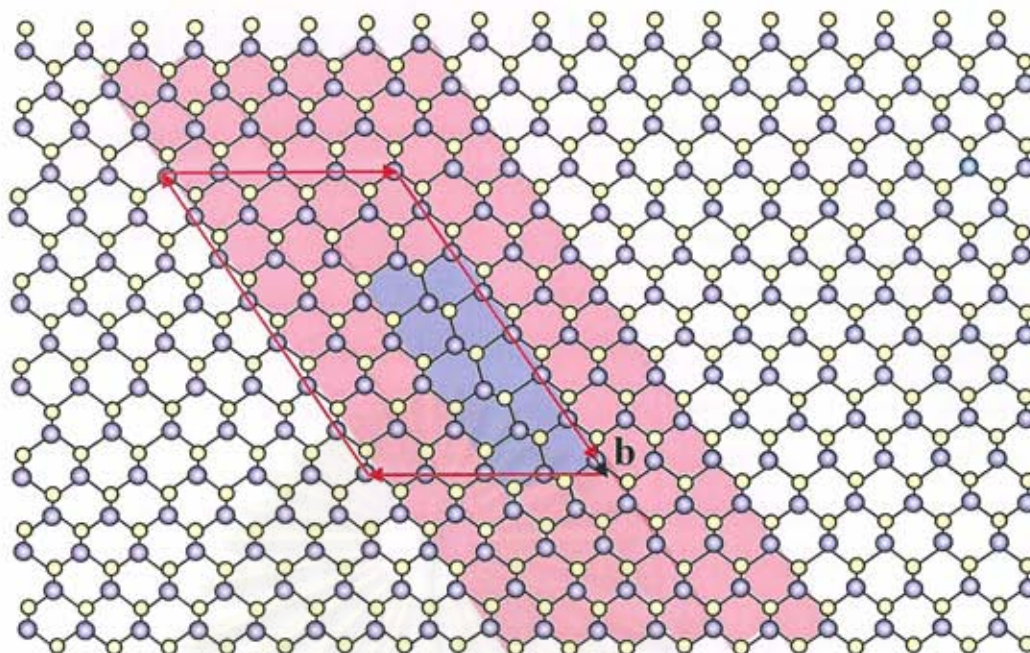
Figure 4.12: Illustration of possible crystal defect in InGaAs buffer layer at (110) cross-section is partial dislocation. The red loop shows burger circuit and black arrow shows burger vector.

shows a schematic of the possible mechanism in atomic scale of stacking fault which end inside the crystal. It is found that when a stacking fault ends inside the crystal, the boundary in the plane fault, separating the faulted region from perfect region of the crystal which produces burger circuit indicated to burger vector (black arrow) unequal to 1 lattice site, is called a partial dislocation.

Next, we consider relieve of strain in this sample. Above-mentioned TDs are generated in first 5 periods of the SLS part due to high contrast, which demonstrated strain relaxation comparing with above part of SLS-InGaAs/GaAs. This suggests that the average composition of 17% In in the SLS part may strongly affect to the generation and confinement of dislocations at the interface region. Although, a few TDs are still propagated in SLS-InGaAs/GaAS, but some of them is end at the SLS-InGaAs/GaAs interface. This is due to different in elastic stiffness constant between InGaAs and GaAs. These results demonstrate an evidence for some filtering of TDs by the SLS due to their bending at the heteroepitaxial interfaces.

4.5 Discussion: A comparison

In general, constant composition buffer layer are useful analysis, e.g. to looking parameter when vary In concentration, but provide no clear advantage in terms of efficient relaxation. For LG-InGaAs layer, there are a large number of dislocations confined at LG-InGaAs which is the origin of strain relaxation. Note that no obvious threading dislocations were observed in the buffer layer. There is a dislocation-free region and fully relaxation in the buffer layer. It is clear that LG technique is suitable for pseudo-substrate. In contrary resulting from SG technique, it is shown that all the CL-layers are under strained owing to less enough layer thickness. Thus, if the buffer layer is grown such SG-InGaAs, it is possible to obtain TDs and residual strain in the buffer layer. On the other hand, the buffer layer on SLS-InGaAs/GaAs exhibits fully relaxed. But, there is a few of stacking fault and partial dislocation thread up in the buffer layer. It is likely that a minority of defect is propagated. The advantage of SLS technique is that SLS help partially confine the TDs within it and relieve residual strain. According to the above results, it is clear that high-quality strain-relaxed InGaAs buffer layer could be achieved by a combination of LG and SLS techniques for the large lattice-mismatched system.

4.6 Summary

In this chapter, microstructures of InGaAs buffer layers grown on GaAs, LG-InGaAs, SG-InGaAs and SLS-InGaAs/GaAs were investigated using TEM technique. The following results concerning microstructural properties were obtained.

(1) The $In_{0.17}Ga_{0.83}As$ layer on GaAs substrate has MDs generated at heteroepitaxial interface due to a large lattice-mismatch. For higher In incorporating $In_{0.27}Ga_{0.73}As$ buffer layer, the growth mode found to be changed from 2D to 3D growth mode. TDs were nucleated by a coalescence of island-like features during the growth. A small number of dislocations in buffer layer is not enough to relieve strain.

(2) The $In_{0.19}Ga_{0.81}As$ buffer layer on LG-InGaAs has both MDs and TDs besides the mixed dislocations and dislocation loops, which are observed in LG-InGaAs part. Possible nucleation of dislocations is in the stage of initial growth and

post growth such as cooling down to room temperature. The results show that the LG technique has the advantage of spreading dislocations with depth throughout LG-InGaAs and must complete full relaxation. The dislocation-free layer was investigated in the buffer layer.

(3) The $In_{0.16}Ga_{0.84}As$ buffer layer on SG-InGaAs shows MDs, TDs and dislocation loops which are generated into the buffer layer. The residual strain still remains in the buffer layer.

(4) The $In_{0.17}Ga_{0.83}As$ buffer layer on SLS-InGaAs/GaAs shows MDs, TDs, partial dislocation and stacking fault, confirming strain-relieved in the SLS region. On the other hand, the SLS technique can be used as a filter of TDs.

Finally, to obtain higher quality buffer layer, a combination of LG and SLS techniques is suggested for fabrication of pseudo-substrate for the large lattice-mismatch system.

CHAPTER V

APPLICATION OF InGaAs BUFFER LAYERS: InGaAsN LAYERS GROWN ON PSEUDO-LATTICE-MATCHED InGaAs SUBSTRATES

To test the quality of the InGaAs pseudo-substrates material qualities of the InGaAsN layers grown on the lattice-matched InGaAs pseudo-substrates were investigated using high resolution X-ray diffraction, transmission electron microscopy, photoluminescence (PL) and photoreflectance (PR). Both optical and structural characteristics of the InGaAsN layer on the lattice-matched InGaAs pseudo-substrate are discussed in comparison to the InGaAsN layer grown directly on the GaAs substrate.

5.1 Overview of InGaAsN on InGaAs

The $In_xGa_{1-x}As_{1-y}N_y$ alloy system is of considerable interest for its potential use as the active layer in the 1.3-1.55 μm wavelength quantum well laser diodes, for which near-lattice-matching to GaAs is possible [13, 45]. This also makes the $In_xGa_{1-x}As_{1-y}N_y$ alloy system interesting for multijunction (MJ) solar cells [46, 47]. Thus, it is challenge to demonstrate thick lattice-matched InGaAsN layers with high optical and structural qualities necessary for the development of the MJ solar cells. In order to decrease the bandgap, it is required to increase the N or In concentrations still further. On one hand, a higher In concentration would increase the compressive strain to a critical point of structural quality of the layer. On the other hand, the incorporation of N will compensate the compressive strain in the layer. However, the larger N concentration is found to degrade the structural and optical properties [48]. Therefore, the lattice mismatch has to be minimized to achieve further improvement of the layer

quality. The use of a graded buffer layer and a strained-layer superlattice in order to provide nearly 100% strain relaxation and reduce the threading dislocation density has produced promising results and has been applied for large lattice mismatched system such as SiGe/Si [49], CuInSe2/InGaAs [50] and InGaAs/GaAs [51], etc.

In this study, such an approach has been applied to the growth of thick $In_xGa_{1-x}As_{1-y}N_y$ with higher In contents. All the $In_xGa_{1-x}As_{1-y}N_y$ layers used in this study were grown by metalorganic vapor phase epitaxy on closely lattice-matched $In_{0.2}Ga_{0.8}As$ layers (InGaAsN/InGaAs) with in-plane lattice mismatch of $\varepsilon_{//} \sim 0.3\%$ at room temperature (RT). The results using various methods such as low-temperature PL, TEM and HRXRD will be discussed in comparison with those of the InGaAsN layers grown directly on GaAs (001) substrates (InGaAsN/GaAs).

5.2 Experimental Procedures

The pesudo-lattice-matched InGaAs substrates (pseudo-substrate) were prepared by MOVPE using trimethylgallium (TMGa), trimethylindium (TMIn) and tertiarybutylarsine (TBAs) as the source materials of Ga, In and As, respectively; the detailed sample structure is shown schematically in Figure 5.1. After a 1.5 μm-thick linearly-graded $In_xGa_{1-x}As$ buffer layer with the final In content of ~20% was deposited, a 900 nm-thick constant $In_{0.2}Ga_{0.8}As$ layer was grown. The gradation is approximated to be 0.8%In/65 nm. This InGaAs composition is chosen so that the InGaAsN layer having the bandgap of 1.0 eV is lattice-matched. Then, a strained-layer superlattice, consists of 10 periods with equal layer thicknesses of $In_{0.2}Ga_{0.8}As$ and GaAs, was grown on the top of the constant $In_{0.2}Ga_{0.8}As$ layer. Finally, a 500 nm-thick constant $In_{0.2}Ga_{0.8}As$ layer was grown as a pseudo-substrate layer.

In the present case, the $In_xGa_{1-x}As_{1-y}N_y$ layers with the In and N contents of $x \sim 0.3$ and $y \sim 0.02$ were grown on both GaAs and $In_{0.2}Ga_{0.8}As$ substrates (Figure 5.1 (a)) by MOVPE using dimethylhydrazine (DMHy) as a N precursor. All the layers were grown at 550°C. The grown layers were characterized by high resolution X-ray diffraction (HRXRD), optical microscopy (OM) and transmission electron microscopy (TEM).
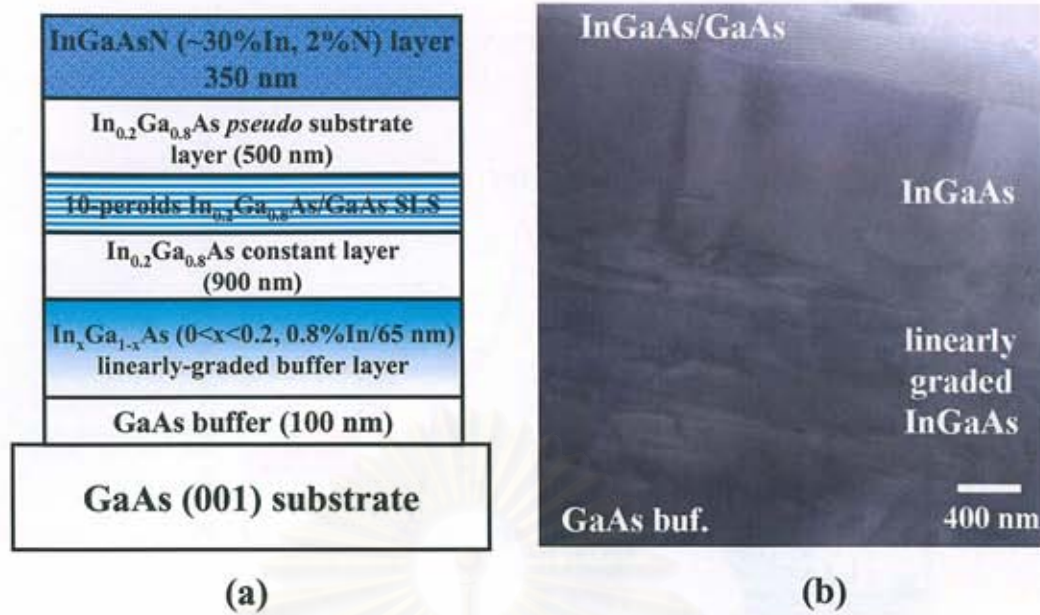
Figure 5.1: Schematic illustration of (a) InGaAsN (~30%In, 2%N) layer on $In_{0.2}Ga_{0.8}As$ pseudo-substrate layer and (b) Cross-sectional <110> bright-field TEM image of the $In_{0.2}Ga_{0.8}As$ pseudo-lattice-matched substrate.

5.3 Strain Relaxation in InGaAsN Layers

Figure 5.2 (a) and (b) shows an x-ray scan in the [001] direction of the InGaAsN (004), InGaAs (004) and GaAs (004) reflections for both (a) GaAs and (b) InGaAs substrates. It is clear from Figure 5.2 (b) that the $In_xGa_{1-x}As_{1-y}N_y$ layer was grown on the pseudo-substrate. As an expectation, an improvement in the full width at half maximum (FWHM) of InGaAsN (004) reflection of InGaAsN/InGaAs (5.2 arcmin) was observed in comparison with that of InGaAsN/GaAs (6.6 arcmin), as shown in Figures 5.2 (b) and (a). In order to evaluate the lattice relaxation precisely, reciprocal lattice mapping of asymmetrical (115) reflection was carried out for the highly lattice-mismatched (InGaAsN/GaAs) and the closer lattice-matched (InGaAsN/InGaAs) layers as shown in Figure 5.3 (a) and (b), respectively. It is clear from Figure 5.3 (a) that both ω-mode and $2\theta/\omega$-mode FWHM from InGaAsN are broaden compared to those from GaAs meaning that the crystal mosaicity and the lattice-coherency in InGaAsN are inferior to those in GaAs. On the other hand, the broadening in ω-mode FWHM from the InGaAsN layer on the pseudo-substrate (Figure 5.3 (b)) is apparently limited by the mosaic of the pseudo-substrate layer.
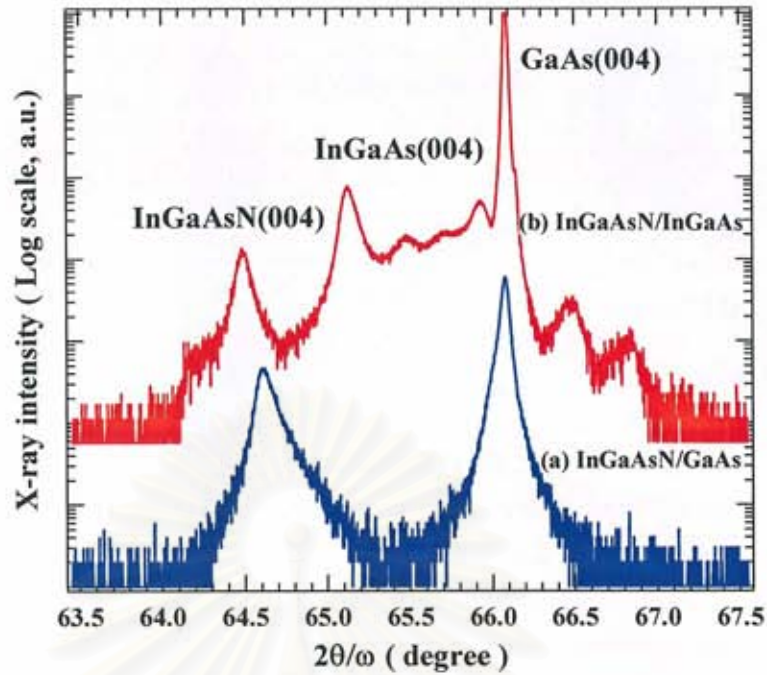
Figure 5.2: High resolution x-ray diffraction (004) curves of $In_{0.3}Ga_{0.7}As_{0.98}N_{0.02}$ (a) on GaAs, and (b) $In_{0.2}Ga_{0.8}As$ pseudo-lattice-matched substrates.

Since the mosaicity in $In_{0.2}Ga_{0.8}As$ pseudo-substrate layer is larger than that of the GaAs substrate, the mosaicity of InGaAsN grown on $In_{0.2}Ga_{0.8}As$ should be also large. However, it is considered to be not sufficient to dominate the film properties. Table 5.1 summarizes the measured lattice parameters of the films perpendicular ($a_{\perp}$) and parallel ($a_{//}$) to the GaAs (001) surface and in-plane lattice-mismatch ($\varepsilon_{//} = \Delta a_{//} / a$). The measured lattice paramenters for InGaAsN show that substantial tensile strain along [001] direction is present in the InGaAsN/GaAs layer. This tensile strain is attributable to an imperfect lattice relaxation at the InGaAsN/GaAs heteroepitaxial interface.

Table 5.1: List of lattice parameters of the InGaAsN films perpendicular ($a_{\perp}$) and parallel ($a_{//}$) to the GaAs (001) surface and in-plane lattice-mismatch ($\varepsilon_{//} = \Delta a_{//} / a$).

Samples	$a_{\perp}$ (Å)	$a_{//}$ (Å)	$a_{sub.}$ (Å)	$\varepsilon_{//}$ (%)
InGaAsN/GaAs	5.767	5.684	5.653[*]	0.55
InGaAsN/InGaAs	5.777	5.747	5.727[**]	0.35

[*] The lattice constant of the GaAs substrate parallel to the (001) surface

[**] The lattice constant of the InGaAs pseudo-substrate layer parallel to the (001) surface
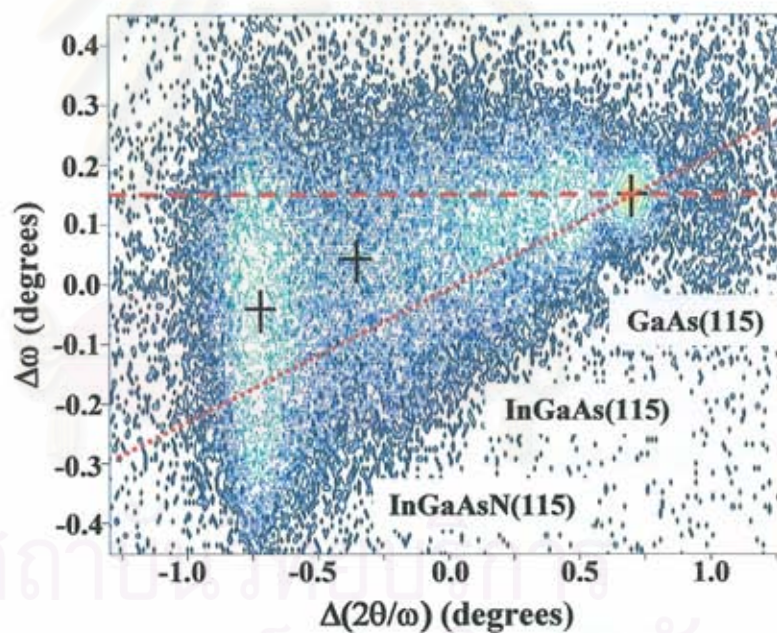
Figure 5.3: Reciprocal space map of the (115) reflection from $In_{0.3}Ga_{0.7}As_{0.98}N_{0.02}$ (a) on GaAs, and (b) $In_{0.2}Ga_{0.8}As$ pseudo-lattice-matched substrates.

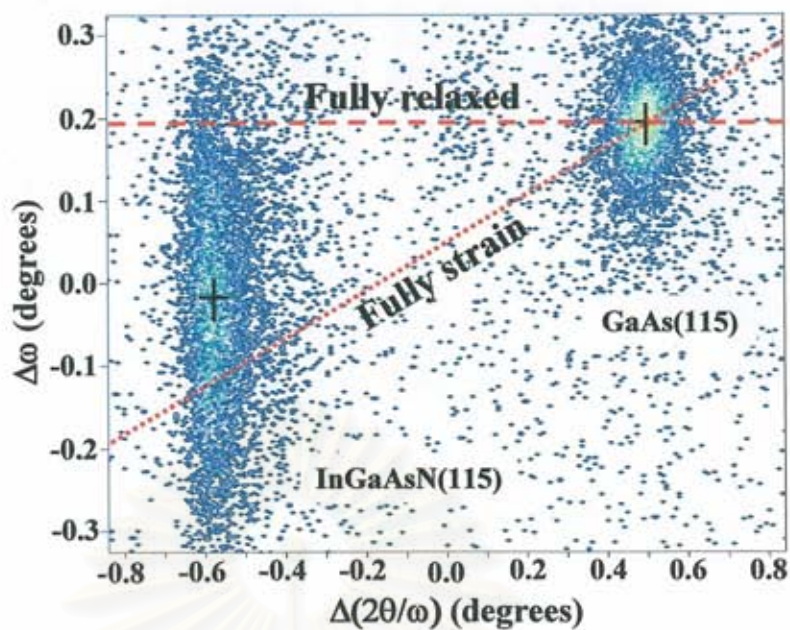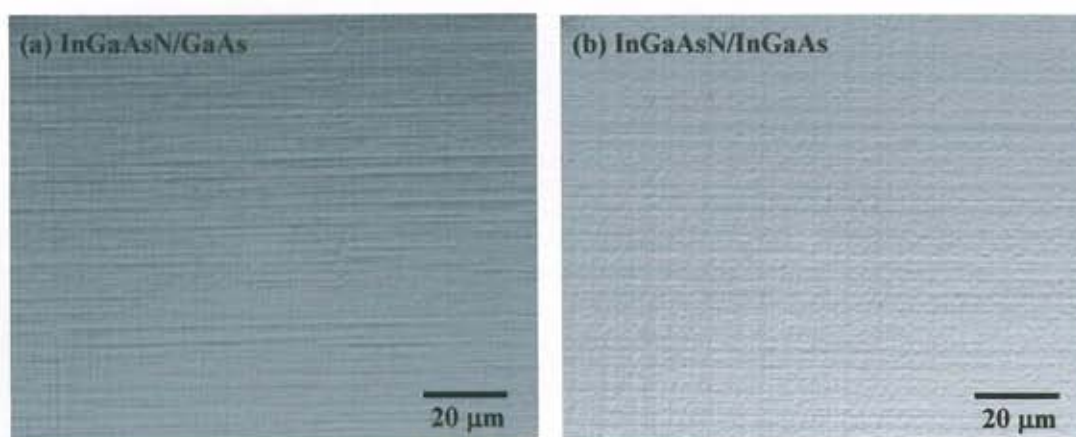**Figure 5.4**: The surface morphologies of $In_{0.3}Ga_{0.7}As_{0.98}N_{0.02}$ (a) on GaAs, and (b) $In_{0.2}Ga_{0.8}As$ pseudo-lattice-matched substrates.

5.4 Surface Morphologies

Figure 5.4 shows surface morphologies of the InGaAsN layers grown on GaAs and $In_{0.2}Ga_{0.8}As$ pseudo-lattice-matched substrates. InGaAsN/InGaAs exhibits cross-hatch morphology oriented approximately (110) and (1-10) cleavege planes with a ridge spacing on the order of ~1 μm (Figure 5.4 (a)). Due to the large lattice-mismatch between $In_{0.2}Ga_{0.8}As_{0.98}N_{0.02}$ and GaAs, we believe this feature is related to the generation of misfit dislocations (MDs) at the InGaAsN/GaAs interface [52]. On the other hand, as shown in Figure 5.4 (b), the morphology undergoes a noticeable change as the pseudo-substrate layer is added. The morphology of InGaAsN/InGaAs shows that the cross-hatch becomes much less dense. It is expected that the number of MDs would be reduced.

5.5 TEM Investigation of InGaAsN Layers

Figure 5.5 (a) shows a cross-sectional TEM image of the InGaAsN layer on the GaAs substrate. It is clearly seen that the MDs, visible by their strain contrast, are located near the InGaAsN/GaAs heteroepitaxial interface (Figure 5.5 (a)). Figure 5.5 (b) shows a cross-sectional TEM image of the InGaAsN layer on the $In_{0.2}Ga_{0.8}As$ pseudo-substrate. It is found that the most of the plastic deformation takes place in the linearly-graded $In_xGa_{1-x}As$ buffer layer. Such large relaxation is enough to isolate
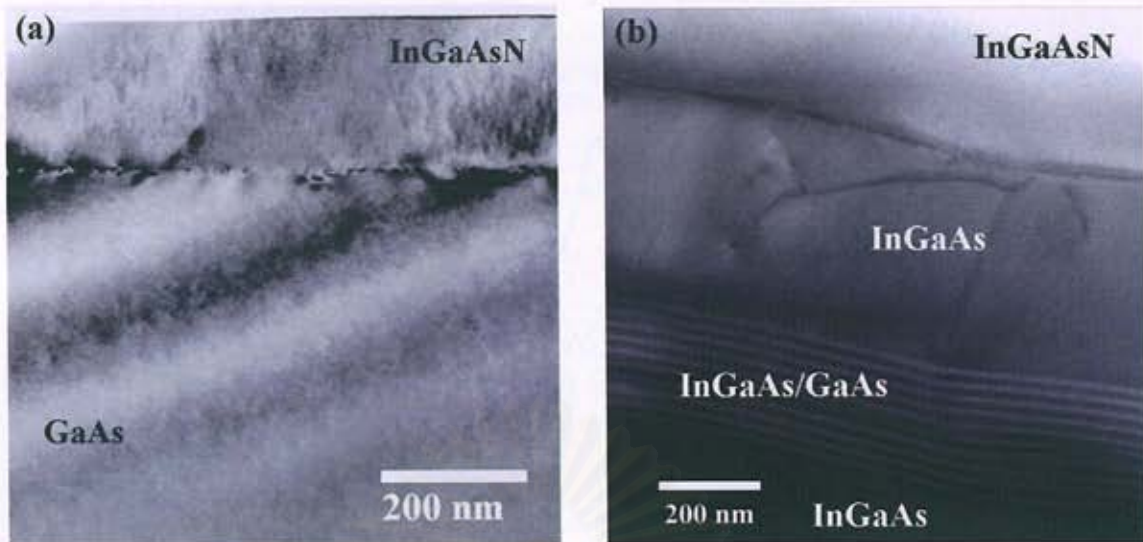
Figure 5.5: Cross-sectional <110> bright-field TEM images of $In_{0.3}Ga_{0.7}As_{0.98}N_{0.02}$ (a) on GaAs, and (b) $In_{0.2}Ga_{0.8}As$ pseudo-lattice-matched substrates.

the upper layers from the GaAs substrate reducing the residual strain in the upper layers. Further, there is also an evidence for some filtering of threading dislocations by the SLS. As an expectation, the number of MDs is significantly reduced in the InGaAsN layer.

5.6 Optical Investigation of InGaAsN layers

Room-temperature PR spectra obtained from InGaAsN/GaAs and InGaAsN/InGaAs are shown in Figure 5.6. We observed the derivative-like spectral feature in PR spectra corresponding to the E_0 transition of the underlying $In_{0.2}Ga_{0.8}As$ at 1.19 eV (Figure 5.6 (b)) and to the transitions at 1.04 (Figure 5.6 (a)) and 1.01 eV (Figure 5.6 (b)), which were attributed to the bandgap of InGaAsN grown on the GaAs and $In_{0.2}Ga_{0.8}As$ substrates, respectively. In addition, in the PR spectrum from InGaAsN/InGaAs, we can see the PR broadening (broadening parameter, Γ) becomes narrower. This implies that the crystal quality of the InGaAsN layer is improved with the addition of the pseudo-substrate layer.

Figure 5.7 shows low-temperature (6 K) PL spectra obtained from InGaAsN/GaAs and InGaAsN/InGaAs. The PL results indicate that the remakable improvement of the InGaAsN quality for InGaAsN/InGaAs is evident from the 5 times increase of the PL intensity and a decrease in PL line width, from 45 meV
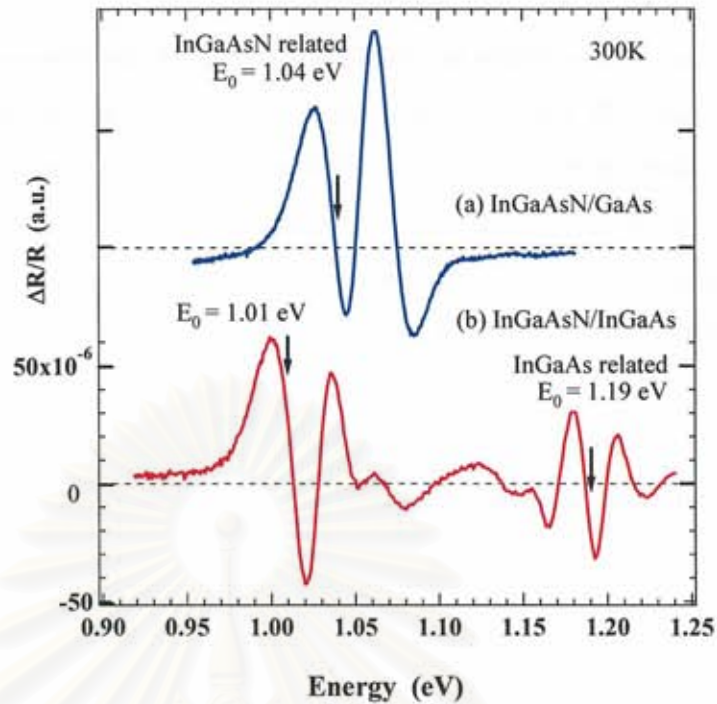
Figure 5.6: Room-temperature PR spectra of $In_{0.3}Ga_{0.7}As_{0.98}N_{0.02}$ on (a) GaAs, and (b) $In_{0.2}Ga_{0.8}As$ pseudo-lattice-matched substrates.
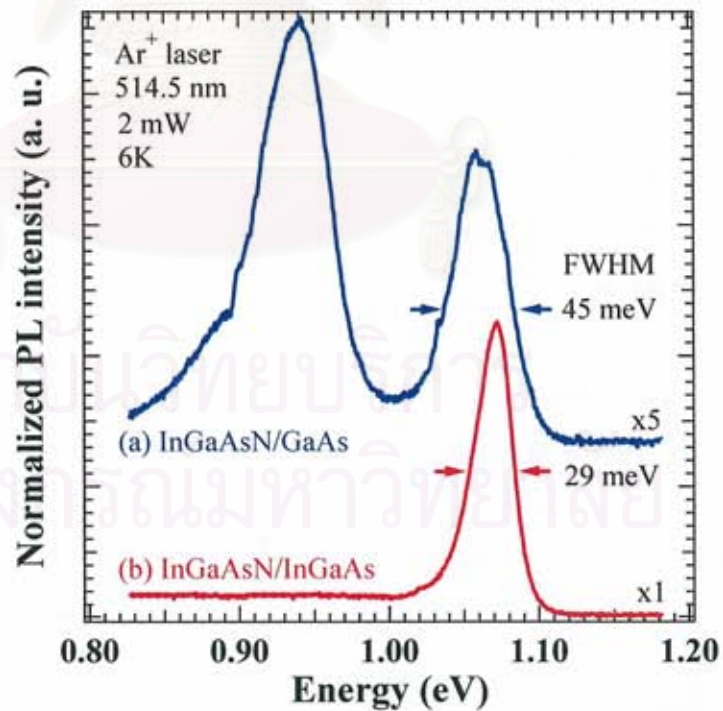
Figure 5.7: Low-temperature (6K) PL spectra of $In_{0.3}Ga_{0.7}As_{0.98}N_{0.02}$ on (a) GaAs, and (b) $In_{0.2}Ga_{0.8}As$ pseudo-lattice-matched substrates.

in InGaAsN/GaAs down to 29 meV in InGaAsN/InGaAs. Unlike InGaAsN/GaAs, the PL spectrum obtained from InGaAsN/InGaAs is excellent with a single near-band-edge emission peak. In addition, it was found that the PL peak intensity of InGaAsN/InGaAs become to be comparable to that of the lower In-content ($x \sim 0.1$) InGaAsN grown lattice-matched to GaAs [53]. This suggests that the InGaAsN top layer has a high structural quality with lower dislocation density. Further improve in the layer quality can make the possible to control the optical property of the high In-content InGaAsN films.

Reduction in the misfit strain though the use of pseudo-substrates made possible the growth of the higher In-content ($x>0.3$) InGaAsN layer with high qualities necessary for the development of the MJ solar cells. Our results also demonstrate that the pseudo-substrate is effective for the reduction of not only the dislocation density but also the nonuniform distribution of In and N which are not detected as the PL (Figure 5.7 (a)) measurement. It is known that these In- and N-rich microscopic regions may act as quantum dots in varied sizes, leading to a long wavelength PL spectrum with broad emission peak [54, 55].

5.7 Summary

We investigated the effectiveness of the pesudo-lattice-matched InGaAs substrate (pseudo-substrate) in improving structural and optical properties of a lattice-mismatched high In-content $In_{0.3}Ga_{0.7}As_{0.98}N_{0.02}$ on GaAs grown by MOVPE. Transmission electron microscopy confirmed that dislocations in InGaAsN on GaAs were effectively reduced with the addition of the InGaAs pseudo-substrate layer. With an insertion of the pseudo-substrate layer, the PL linewidth was reduced from 45 meV to 29 meV and PL intensity was comparable to the lower In-content InGaAsN grown lattice-matched to GaAs. Our results are encouraging for the application the pseudo-lattice-matched InGaAs substrate to lattice-mismatched system and high In-content InGaAsN on GaAs to extend the wavelength of InGaAsN material.

CHAPTER VI
CONCLUSIONS

In this thesis, the structural properties of the MOVPE grown $In_xGa_{1-x}As$ buffer layers on (i) GaAs, (ii) linearly-graded (LG) InGaAs layer, (iii) step-graded (SG) InGaAs layer and (iv) strain-layer superlattice (SLS) InGaAs/GaAs were investigated. Transmission electron microscopy (TEM) was mainly used to characterize the structural defects, including misfit (MD), threading (TD) and mixed type dislocations. In order to examine lattice parameters and strain properties, high resolution X-ray diffraction (HRXRD) measurements were carried out.

Our results show that the generation of dislocations (MDs, TDs and mixed type dislocations) investigated by cross-sectional TEM was found to be dominated in the LG-InGaAs regions. This means that the LG-InGaAs regions were relaxed due to the large lattice-mismatch between InGaAs and GaAs, resulting in generation of a large number of dislocations. On the other hand, for the SLS-InGaAs buffer layer, a high density of dislocations was observed in the InGaAs/GaAs superlattice regions. In fact, density of dislocations was decreased in the InGaAs buffer layer (top layer) grown on the InGaAs/GaAs superlattice. This demonstrates that the strained-layer superlattice exhibits some filtering of threading dislocations. Also, the comparison of the strain-relaxation in the InGaAs buffer layers grown on GaAs, LG-, SG- and SLS-InGaAs layers is discussed.

These results demonstrate that the majority of structural defects in all the buffer layers are dislocations. It is found that the dislocations are mainly caused by the strain-relaxation in the InGaAs buffer layers. Thus, we demonstrate that a combination of the LG and SLS techniques is a promising method to achieve high-quality strain-relaxed InGaAs buffer layers for the growth of lattice-matched system, especially InGaAsN/InGaAs.

References

[1] F. Romanto, E. Napolitani, A. Carnera, A. V. Drigo, L. Lazzarini, G. Salviati, C. Ferrari, A. Bosacchi and S. Franchi. Strain relaxation in graded composition $In_xGa_{1-x}As/GaAs$ buffer layers. *J. Appl. Phys.* **86** (1999): 4748-4755.

[2] M. S. Abrahams, L. R. Weisberg, J. Blanc, and C. J. Buiocchi. Dislocation morphology in graded heterojunctions: $GaAs_{1-x}P_x$. *J. Mater. Sci.* **4** (1969): 223-235.

[3] M. S. Abrahams, J. Blanc, and C. J. Buiocchi. Like-sign asymmetric dislocations in zinc-blende structure. *Appl. Phys. Lett.* **21** (1972): 185-186.

[4] F. K. LeGoues, B. S. Meyerson, and J. F. Morar. Anomalous strain relaxation in SiGe thin films and superlattices. *Phys. Rev. Lett.* **66** (1991): 2903-2906.

[5] D. J. Eaglesham and M. Cerullo. Dislocation-free Stranski-Krastanow growth of Ge on Si (100). *Phys. Rev. Lett.* **64** (1993): 1943-1946.

[6] M. Berti, A. V. Drigo, G. Rossetto, and G. Torzo. Experimental evidence of two-dimensional-three-dimensional transition in the Stranski–Krastanow coherent growth. *J. Vac. Sci. Technol. B* **15**, (1997): 1794-1799.

[7] M. Tamura, A. Hashimoto and Y. Nakatsugawa. Threading dislocations in $In_xGa_{1-x}As/GaAs$ heterostructures. *J. Appl. Phys.* **72** (1992): 3398-3405.

[8] P. Kidd, D. J. Dunstan, H. G. Colson, M. A. Lourenço, A. Sacedón, F. González-Sanz, L. González, Y. González, R. García, D. González, F. J. Pacheco and P. J. Goodhew. Comparison of the crystalline quality of step-graded and continuously graded InGaAs buffer layers. *J. Cryst. Growth* **169** (1996): 649-659.

[9] R. Beanland, D. J. Dunstan and P. J. Goodhew. Plastic relaxation and relaxed buffer layers for semiconductor epitaxy. Review. *Adv. Phys.* **45** (1996): 87-146.

[10] D. J. Dunstan, S. Young and R. H. Dixon. Geometrical theory of critical thickness and relaxation in strain-layer growth. *J. Appl. Phys.* **70** (1991): 3038-3040.

[11] J. Tersoff. Dislocations and strain relief in compositionally graded layers. *Appl. Phys. Lett.* **62** (1993): 693-695.

[12] P. Kongjaeng, S. Sanorpim, T. Yamamoto, W. Ono, F. Nakajima, R. Katayama

and K. Onabe. Structural investigation of InGaAsN films grown on pseudo-lattice-matched InGaAs substrates by metalorganic vapor phase epitaxy. *J. Cryst. Growth* **298** (2007): 111-115.

[13] M. Kondow, T. Kitatani, S. Nakatsuka, M. C. Larson, K. Nakahara, Y. Yazawa and M. Okai. GaInNAs: A novel material for long-wavelength semiconductor lasers. *IEEE J. Select. Topics Quantum Electron.* **3** (1997): 719-730.

[14] L. Hae-seok, K. Nishimura, Y. Yagi, M. Tachibana, N. J. Ekins-Daykes, Y. Ohshita, N. Kojima and M. Yamaguchi. Chemical beam epitaxy of InGaAsN films for multi-junction tandem solar cells. *J. Cryst. Growth* **275** (2005): e1127-e1130.

[15] Bullough T. J., Davies S., Thomas S., Joyce T. B. and Chalker P. R. Effect of increased nitrogen incorporation on the growth of GaInNAs/GaAs. *Solid-State Electronics* **47** (2003): 407-412.

[16] Sanorpim S., Nakajima F., Imura S., Katayama R., Wu J., Onabe K. & Shiraki Y. Physical mechanisms of photoluminescence of InGaAs(N) alloy films grown by MOVPE. *phys. stat. sol. (b)* **234** (2002): 782-786.

[17] A. Sacedón, F. González-Sanz, E. Calleja, E. Muñoz, S. I. Molina, F. J. Pacheco, D. Araújo, R. García M. Lourenço, Z. Yang, P. Kidd, and D. Dunstan, Design of InGaAs linear graded buffer structures. *Appl. Phys. Lett.* **66** (1995): 3334-3336.

[18] Milton Ohring. *The Materials Science of Thin Films.* London: Academic Press, Inc., 1992.

[19] D. Hull and D. J. Bacon. *Introduction to Dislocations.* 3rd ed. England: Pergamon Press Ltd., 1984.

[20] H. Klapper. Generation and propagation of dislocations during crystal growth. *Mater. Chem. and Phys.* **66** (2000): 101-109.

[21] V. I. Vdovin. Nature and origin of pure edge dislocations in low mismatched epitaxial structures. *J. Cryst. Growth* **172** (1997): 58-63.

[22] R. Hull and J. C. Bean. Variation of misfit dislocation behavior as a function of strain in the GeSi/Si system. *Appl. Phys. Lett.* **54** (1989): 925-927.

[23] R. G. Hongland, J. P. Hirth, A. Misra, and D. Mitlin. Influence of surface step on glide of threading dislocations during layer growth. *Appl. Phys. Lett.* **84** (2004): 5136-5138.

[24] O. Yastrubchak, T. Wosinski, T. Figielski, E. Lusakowska, B. Pecz and A. L. Toth. Misfit dislocations and surface morphology of lattice-mismatched GaAs/InGaAs heterostructures. *Physica E* **17** (2003): 561-563.

[25] A. H. Herzog, D. L. Keune and M. G. Craford. High-efficiency Zn-diffused GaAs electroluminescent diodes. *J. Appl. Phys.* **43** (1972): 600-602.

[26] G. H. Olsen. Interfacial lattice mismatch effects in III-V compound. *J. Cryst. Growth* **31** (1975): 223-239.

[27] C. A. B. Ball and C. Laird. A calculation of the energy of misfit dislocations and the critical thickness in graded epitaxial layers. *Thin Solid Films* **41** (1977): 307-314.

[28] G. H. Olsen, M. S. Abrahams, C. J. Buiocchi, and T. J. Zamerowski. Reduction of dislocation densities in heteroepitaxial III–V VPE semiconductors. *J. Appl. Phys.* **46** (1975): 1643-1646.

[29] G. A. Rozgonyi and M. B. Panish. Stress compensation in $Ga_{1-x}Al_xAs_{1-y}P_y$ LPE layers on GaAs substrates. *Appl. Phys. Lett.* **23** (1973): 533-535.

[30] G. A. Rozgonyi, P. M. Petroff and M. B. Panish. Control of lattice parameters and dislocations in the system $Ga_{1-x}Al_xAs_{1-y}P_y$/GaAs. *J. Cryst. Growth* **27** (1974): 106-117.

[31] C. A. B. Ball and J. H. Van Der Merwe. *The Growth of Dislocation-free Layers*, North-Holland Publishing Company, 1983.

[32] K. Uesugi, N. Morooka and I. Suemune. Reexamination of N composition dependence of coherently grown GaNAs band gap energy with high-resolution X-ray diffraction mapping measurements. *Appl. Phys. Lett.* **74** (1999): 1254-1256.

[33] David R. Lide. *CRC Handbook of Chemistry and Physics.* 85th ed. New York: National Institute of Standards on Technology, 2004-2005.

[34] M. H. Loretto. *Electron Beam Analysis of Materials.* 2nd ed. London: Chapman-Hall, 1994.

[35] David B. Williams and C. Barry Carter. *Transmission Electron Microscopy: A Textbook for Materials Science.* New York: A Division of Plenum publishing Corporation, 1996.

[36] K. H. Chang, R. Gibala, D. J. Srolovitz, P. K. Bhattacharya and J. F. Mansfield. Crosshatched surface morphology in strained III-V semiconductor films. *J. Appl. Phys.* **67** (1990): 4093-4098.

[37] R. A. Burmeister, G. P. Pighini and P. E. Greene, Trans. *TMS-AIME* **245** (1969): 587.

[38] T. Nishioka, Y. Itoh, A. Yamamoto and M. Yamaguchi. Crosshatch patterns in GaAs films on Si substrates due to thermal strain in annealing processes. *Appl. Phys. Lett.* **51** (1987): 1928-1930.

[39] A. Salokatve and M. Hovinen. The effect of strain on morphology and structural properties of InGaAs/InP (001) grown by molecular beam epitaxy. *J. Appl. Phys.* **67** (1990): 3378-3381.

[40] Y. Meeyoung, L. Bun, B. Jong-Hyeob, P. Hyo-Hoon and L. El-Hang. Evolution of the surface cross-hatch pattern in $In_xGa_{1-x}As$/GaAs layers grown by metal-organic chemical vapor deposition. *Appl. Phys. Lett.* **68** (1996): 16-18.

[41] A. Trampert and K. H. Ploog. Heteroepitaxy of Large-Misfit Systems: Role of Coincidence Lattice. *Cryst. Res. Technol.* **35** (2000): 793-806.

[42] S. Chang, T. Chang and S. C. Lee. The growth of highly mismatched $In_xGa_{1-x}As$ ($0.28 \leq x \leq 1$) on GaAs by molecular-beam epitaxy. *J. Appl. Phys.* **73** (1993): 4916-4926.

[43] Ch. Jäger, E. Spiecker, J. P. Morniroli and W. Jäger. Analysis of dislocation loops by means of large-angle convergent beam electron diffraction. *J. Phys: Condens. Matter* **14** (2002): 12777-12782.

[44] Siripen Suandon. *Structural property analysis of GaN grown on GaAs by MOVPE using transmission electron microscopy.* Master's thesis, Graduate School, Chulalongkorn University, 2005, p. 29.

[45] M. Weyer, M. Sato and H. Ando. Red shift of Photoluminescence and Absorptin in Dilute GaAsN Alloy Layers. *Jpn. J. Appl. Phys.* **31** (1992): L853-L855.

[46] M. Kondow, T. Kitatani, K. Nakahara and T. Tanaka. A 1.3 µm GaInNAs laser diode with a lifetime of over 1000 hours. *Jpn. J. Appl. Phys.* **38** (1999): L1355-L1356.

[47] S. R. Kurtz, A. A. Allerman, E. D. Jones, J. M. Gee, J. J. Banas and B. E. Hammons. InGaAsN solar cell with 1.0 eV band gap, lattice matched to GaAs. *Appl. Phys. Lett.* **74** (1999): 729-731.

[48] T. J. Bullough S. Davies, S. Thomas, T. B. Joyce and P. R. Chalker. Effect of increased nitrogen incorporation on the growth of GaInNAs/GaAs. *Solid-State Electronics* **47** (2003): 407-412.

[49] E. A. Fitzgerald et al. Totally relaxed Ge_xSi_{1-x} layers with low threading dislocation grown on Si substrate. *Appl. Phys. Lett.* **59** (1991): 811-813.

[50] S. Niki, P. J. Fons, A. Yamada, T. Kurafuji, S. Chichibu, H. Nakanishi, W. G. Bi and C. W. Tu. High quality $CuInSe_2$ films grown on pseudo-lattice-matched substrates by molecular beam epitaxy. *Appl. Phys. Lett.* **69** (1996): 647-649.

[51] D. E. Aspnes. Third-derivative modulation spectroscopy with low-field electroreflectance. *Surf. Sci.* **37** (1967): 418-442.

[52] W. K. Cheah, W. J. Fan, S. F. Yoon, S. Z. Wang and W. K. Loke, X-ray reciprocal space mapping of strain relaxation in $GaAs_{1-x}N_x$ on GaAs[100] by molecular-beam epitaxy. *J. Appl. Phys.* **94** (2003): 3828-3833.

[53] S. Sanorpim, F. Nakajima, W. Ono, R. Katayama, and K. Onabe. High-nitrogen-content InGaAsN films on GaAs grown by metalorganic vapor phase epitaxy with TBAs and DMHy. *phys. stat. sol. (a)* **203** (2006): 1612-1617.

[54] F. Nakajima, S. Sanorpim, T. Yamamoto, E. Takuma, R. Katayama, H. Ichinose, K. Onabe and Y. Shiraki, Microstructures, defects, and localization luminescence in InGaAsN alloy films. *phys. stat. sol. (c)* **0** (2003): 2778-2781.

[55] H. P. Xin, K. L. Kavanagh, Z. Q. Zhu, and C. W. Tu. Quantum dot-like behavior of GaInNAs/GaAs quantum wells grown by gas-source molecular-beam epitaxy. *J. Vac. Sci. Technol. B* **17** (1999): 1649-1653.

Vitae

Miss Pornsiri Kongjaeng was born on June 23, 1982 in Chachoengsao, Thailand. She received her Bachelor of Science in Physics from King Mongkut's University of Technology Thonburi in 2003, and continued her Master degree study at Chulalongkorn University.

Publications and Conference Presentations:

1. **P. Kongjaeng**, S. Sanorpim, T. Yamamoto, W. Ono, F. Nakajima, R. Katayama and K. Onabe, 'Structural investigation of InGaAsN films grown on pseudo-lattice-matched InGaAs substrates by metalorganic vapor phase epitaxy', *Journal of crystal growth*, 298 (2007): 111-115.

2. **Pornsiri Kongjaeng**, Sakuntam Sanorpim, Takahisa Yamamoto, Wataru Ono, Fumio Nakajima, Ryuji Katayama and Kentaro Onabe, 'Structural investigation of InGaAsN films grown on pseudo-lattice-matched InGaAs substrates by metalorganic vapor phase epitaxy' *13th International Conference on Metal Organic Vapor Phase Epitaxy*, Japan, May 22-25, 2006.

3. **Pornsiri Kongjaeng**, Sakuntam Sanorpim, Takahisa Yamamoto, Wataru Ono, Fumio Nakajima, Ryuji Katayama and Kentaro Onabe, 'Comparison of the structural quality of InGaAsN films grown on InGaAs pseudosubstrate and on GaAs substrates' *14th Acadamic Conference*, Faculty of Science, Chulalongkorn University, Thailand, March 16-17, 2006.

4. **Pornsiri Kongjaeng**, Sakuntam Sanorpim, and Kentaro Onabe, 'Comparison of structural properties of linear graded and strain-layer-superlattice InGaAs buffer layers' *32nd Congress on Science and Technology of Thailand* , Chulalongkorn University, Thailand, October 10-12, 2006.

5. **Pornsiri Kongjaeng**, Sakuntam Sanorpim, Takahisa Yamamoto, Wataru Ono, Fumio Nakajima, Ryuji Katayama and Kentaro Onabe, 'Material quality of InGaAsN films Grown on InGaAs pseudosubstrate by metalorganic vapor phase epitaxy' *The 6th National Symposium on Graduate Research*, The Graduate School, Chulalongkorn University, Thailand, October 13-14, 2006.

6. **Pornsiri Kongjaeng**, Sakuntam Sanorpim and Kentaro Onabe, 'Micro-structural characterization of linear graded and strain-layer superlattice InGaAs buffer layers' *The 24th Microscopy Society of Thailand*, Kasedsard University, Thailand, February 14-16, 2007.